Meteoritics & Planetary Science 37, 623–647 (2002)
Available online at http://www.uark.edu/meteor

Mineralogy and petrology of melt rocks from the Popigai impact structure, Siberia

J. WHITEHEAD[1]*, R. A. F. GRIEVE[2] AND J. G. SPRAY[1]

[1]Planetary and Space Science Centre, Department of Geology, University of New Brunswick, Fredericton, New Brunswick E3B 5A3, Canada
[2]Earth Sciences Sector, Natural Resources Canada, Ottawa, Ontario K1A OE4, Canada
*Correspondence author's e-mail address: jwhitehe@unb.ca

(Received 2001 August 1; accepted in revised form 2002 January 24)

Abstract–The late Eocene Popigai impact structure of Siberia comprises an approximately 0.5–1.5 km thick, ~100 km diameter sequence of clast-rich and clast-poor andesitic to rhyolitic impact melt rocks and impact breccias, underlain by Archean to Proterozoic crystalline basement and Proterozoic to Phanerozoic sedimentary rocks. The fine-grained to cryptocrystalline texture of the more melt-rich rocks, despite their occurrence in bodies locally in excess of 800 m thick and 28 km long, suggests that the melt crystallized in response to (1) cooling by the clast load, and/or; (2) rapid nucleation on finely brecciated clasts, which have since been assimilated and/or; (3) crystallization enhanced by the relatively low water contents of the melts. Rapid crystallisation of the melt is indicated by the lack of zoning in minerals, the presence of glass, the lack of strain recovery features in clasts and the lack of evidence for fractionation in the major and trace elements, including the rare earth elements. Optical and analytical electron microscopy reveal that the previously reported division of the melt rocks into high- and low-temperature variants based on hand sample appearance, or glass content, is not warranted.

Clasts within the melt-rich rocks exhibit a wide range of shock metamorphic features, though they are not distributed in the impact melts in a systematic manner. This indicates that the melt-rich rocks were well mixed during their formation, thus juxtaposing unshocked with shocked material. Injection of mesostasis melt into partially melted checkerboard plagioclase and orthopyroxene clasts also occurred during this mixing stage.

INTRODUCTION

The late Eocene Popigai meteorite impact structure is located in northern Siberia (latitude 71°30' N, longitude 111°1' E; Fig. 1 and insert). Popigai has a diameter of ~100 km and, along with Manicouagan is currently the world's joint fourth largest impact structure, exceeded only in size by Vredefort, Chicxulub and Sudbury (Grieve *et al.*, 1995). Popigai represents the least-eroded, exposed example of a terrestrial peak ring impact basin. Other known examples are eroded (Manicouagan, Vredefort), buried (Chesapeake Bay, Chicxulub), or tectonized (Sudbury). The entire structure is well-preserved, from brecciated basement, through various breccias, impact melt rocks, to post-impact sedimentary rock cover (Masaitis, 1994).

Detailed studies of impact-generated melt rocks and their clast content can reveal (1) information about the behavior of the target during impact, (2) the pressures and temperatures achieved during impact, and (3) the cooling and crystallisation history of the melt rocks. This work characterizes the textural and geochemical attributes of the melt rocks and their clast content at Popigai in order to assess which of these factors are correlated, and to interpret their cooling-crystallisation history in the context of post-impact dynamics.

GEOLOGICAL SETTING

The target lithologies of the Popigai impact structure comprise Archean and Proterozoic crystalline rocks that are overlain by a gently northeast-dipping sequence of sedimentary rocks that range from a thickness of zero in the southwest portion of the structure to a maximum of 1 km beneath the northeast rim (Masaitis, 1994) (Fig. 1). The sedimentary units comprise Proterozoic to Cambrian conglomerates, quartzites, dolomites and limestones, Permian terrestrial sandstones and argillites, and Cretaceous reworked sands and sedimentary rock. Triassic diabase sills have locally intruded rocks to the northeast of the impact structure (Masaitis, 1994).

Popigai is a complex crater with a central depression 2.0–2.5 km deep, an annular uplift ~45 km in diameter and an outer annular trough 15 to 18 km wide and 1.2–2.0 km deep (Masaitis *et al.*, 1980; Masaitis,1994). The structure is filled with breccias containing <10 vol% melt-clasts (allogenic breccia), melt clast-rich breccias (so-called suevite) and clast-bearing

Prelude preprint MS#4617

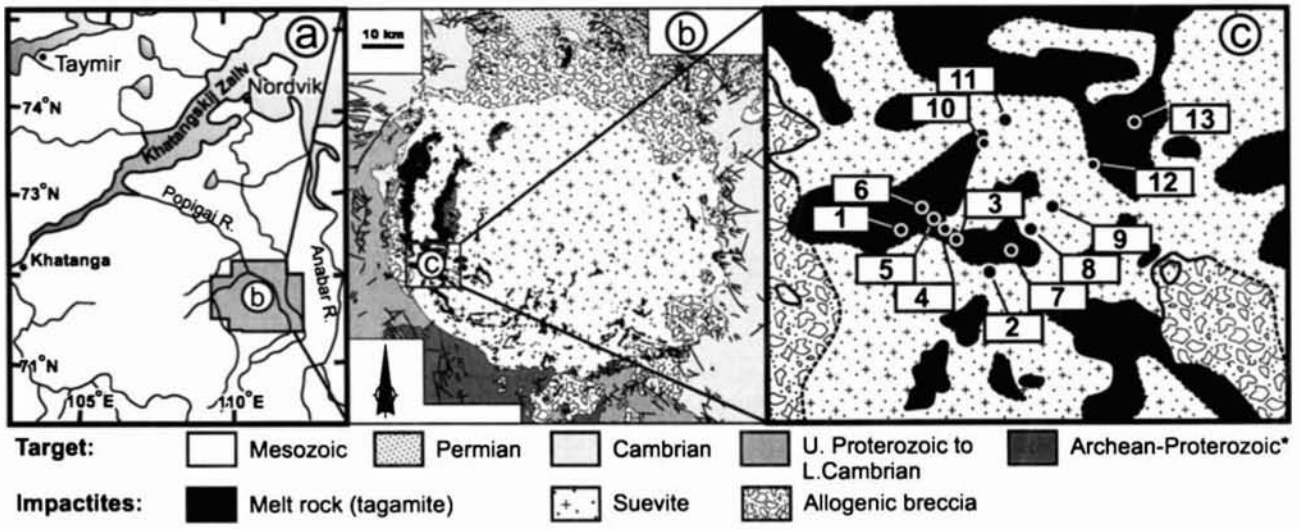

FIG. 1. (a) Location map; (b) and (c) bedrock geology maps of the Popigai impact structure modified from the unpublished compilation of V. L. Masaitis. Map (c) shows the location of the drill sites from which the samples in this study were collected. The on-site borehole numbering system is as follows: 1 = 4274; 2 = 4650; 3 = 4662; 4 = 4666; 5 = 4670; 6 = 4674; 7 = 5050; 8 = 5450; 9 = 5850; 10 = 5874; 11 = 6274; 12 = 6650; and 13 = 7450. The insert fold-out color geology map in this issue presents a more detailed subdivision of the lithological units than previously available, draped over a digital terrain model showing the paths of principal rivers.

impact melt rocks. These collectively achieve thicknesses of 1.5 km. Outliers of allogenic breccia extend up to 30 km outside the original crater rim (Masaitis *et al.*, 1980). The presence of shatter cones, multiple planar deformation features (PDFs) in quartz and other shock features unequivocally attest to an impact origin for the Popigai structure (Grieve *et al.*, 1996; French, 1998).

The impact melt rocks outcrop predominantly in the western and southern quadrants of the impact structure (Fig. 1). They are known locally as tagamites, after their type locality in the Tagamy Hills in the west of the structure (Masaytis *et al.*, 1972). The melt rocks occur as irregular bodies, small lenses and dyke-like bodies in the suevites, and in the allogenic breccias as lenses (Masaitis, 1994; Vishnevsky and Montanari, 1999). The melt rocks are located in the west of the structure between the underlying allogenic breccias and overlying suevites as sub-horizontal lensoid bodies up to 780 m thick and 32 km long. Melt rocks are also located 15 km southwest of the continuous outcrop of the impactites, lying directly on the basement gneisses (Masaitis *et al.*, 1980). The melt rocks yield $^{40}Ar/^{39}Ar$ step-heating age of 35.7 ± 0.2 Ma, which is the best constraint on the timing of the impact (Bottomley *et al.*, 1997).

The presence of impact-generated diamonds in the structure stimulated the collection of over 130 km of drill core, principally from the melt rock units, from more than 700 boreholes since the 1970s (Masaitis *et al.*, 1972; Koeberl *et al.*, 1997). Samples for this study were taken from 13 of these cores (Fig. 2).

ANALYTICAL TECHNIQUES

Major element spot analyses were determined, at the University of New Brunswick (UNB), on a JEOL 733 electron microprobe at an accelerating potential of 15 kV, a current of 10 nA and a peak-count duration of 30 to 40 s, using wavelength dispersive spectrometers. Loss of volatile alkali elements (Na and K) was minimized during analysis by peak counting for these elements before the less volatile elements. Bulk melt rock analysis was performed by the Analytical Chemistry Section of the Geological Survey of Canada. Major elements were determined by x-ray fluorescence spectroscopy (XRF) and trace elements by inductively coupled plasma-mass spectrometry (ICP-MS). H_2O, CO_2 and S contents were obtained by sample combustion at 1300 °C in the presence of V_2O_5 by infrared detection or, in the case of H_2O, using a LECO RMC-100 moisture determinator. Minute samples of metallic Fe were detected, most likely derived from the crushing apparatus at Khatanga, Siberia, where the powdered samples were prepared, following XRF analysis. Compositional analysis of the filings indicate a composition of pure Fe with trace amounts of Mn (0.64 wt%), Si (0.59 wt%) and Cu (0.17 wt%). The siderophiles Co and Ni do not occur above their detection limit (0.3 wt%), while Cr occurs in quantities (0.20 wt%) which are only marginally above the detection limit for this element (0.19 wt%). The low abundance (<<0.1 wt%) of the filings and their pure Fe composition will not, therefore, have significantly affected the major or trace element compositions of the melt rocks.

Glass clasts in the melt rock were separated using a vibrating tool. Pure-glass chips were isolated by hand under the binocular microscope. The samples were leached and analysed at the Isotope Laboratory of Caltech following the methods outlined in Stecher *et al.* (1989) and Whitehead *et al.* (2000), respectively.

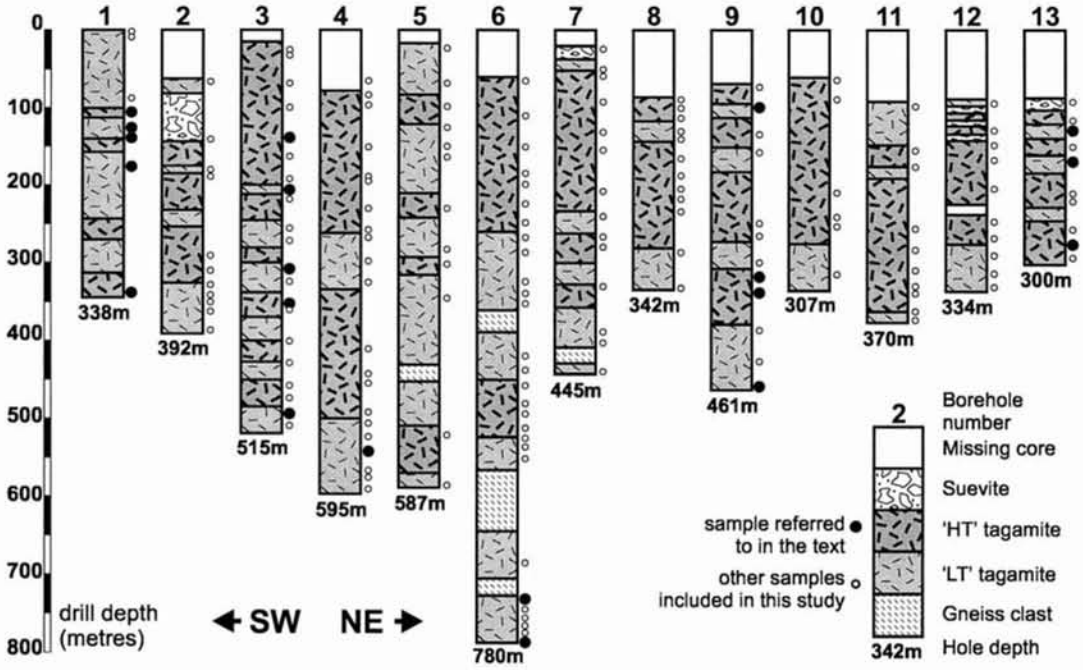

FIG. 2. The 13 drill cores sampled for this study, showing the previously suggested subdivisions into so-called high-temperature (HT) and low-temperature (LT) impact melt rocks (tagamites) based on hand sample observation of the core samples. Drill site locations are presented on Fig. 1. Although the samples are not taken along a single linear transect, the order of the cores in the figure broadly reflects an increase in distance from the crater centre, with increasing core number.

We accurately measured the clast content and clast sizes on scanned photomicrographs of the samples in which the margin of all clasts >0.2 mm in diameter had been manually defined using an image analysis program (Scion Image). Clasts smaller than 0.2 mm in diameter are unrepresented by our data, owing to our inability to accurately define their boundaries and distinguish them from groundmass phases. The mean of the longest and shortest clast diameters are reported for non-equant examples. The groundmass grain size and the width of reaction coronas that occur around quartz clasts in the melt rocks were measured using the imaging systems on UNB's electron microprobe and JEOL 6400 analytical scanning electron microscope (ASEM). The mean groundmass grain size was established using 10 to 15 measurements of the shortest diameter of random crystals from each sample. Digital backscattered electron images, x-ray compositional maps and the distribution of the volatile phases were obtained using the ASEM, the latter with the Be window removed.

The low-density, high-temperature silica polymorphs cristobalite and tridymite were concentrated from crushed melt rock samples using the heavy liquid methylene iodide. X-ray diffraction analysis was performed on multi-crystal aggregates using a Debye-Scherrer camera fitted with a Gandolfi attachment. Monochromatic CuKα x-rays were generated by a modified Philips 1710 diffractometer. X-ray intensities and counts were measured using a gas proportional detector at incident angles of 5 to 85° at counting steps of 0.02°.

MINERALOGY AND PETROLOGY

Groundmass

The degree of crystallinity of the matrix of the impact melt rocks varies from almost completely crystalline to clear-brown glass containing ~10 vol% crystals. The majority of samples possess >60 vol% crystals, which comprise fine-grained (1 to 100 μm grain size) prismatic, euhedral to subhedral enstatite ($En_{52-58}Fs_{38-47}Wo_{1-7}$) and euhedral to subhedral plagioclase ($An_{42-66}Ab_{32-52}Or_{1-9}$) with intersertal glass ± potassic feldspar. Accessory phases include prismatic ilmenite and local subhedral to euhedral acicular hercynite (*e.g.*, sample 9-340). Rounded, immiscible globules of pyrrhotite ($Fe_{1-x}S$, where $x = 0.91$ to 0.94), up to 0.75 mm in diameter, are present locally. Although the pyroxenes contain predominantly low CaO (<1 wt%, <2% Wo), one grain possesses 3.4 wt% CaO (7.2% Wo).

Fan spherulites (trichites) occur in some of the glass-dominated melt rocks. These radiating acicular crystals have not preferentially nucleated on any particular clast type. The narrow dimension of the crystallites (~1 μm) preclude an accurate determination of their composition using the electron microprobe. Nevertheless, they appear to have an alkali feldspar composition.

Brown to colorless interstitial and patchy matrix glasses possess overlapping compositional ranges. However, in individual samples, the brown glasses contain significantly

higher MgO and FeO and lower SiO_2 contents than colorless glasses. Euhedral to subhedral equant cordierite crystals are present in the most glassy samples (*e.g.*, 4-550).

Clasts

The attributes of clasts within samples subdivided into "high-temperature" (HT) and "low-temperature" (LT) melt rocks, based on their inferred initial temperatures (Masaitis, 1994; Masaitis *et al.*, 1998), are presented in Table 1. The merit of the HT/LT subdivision, which is based on the relative abundance of glass in the samples, is evaluated below. The melt rocks contain clast loads that vary from 1.0 to 35.5 vol% in the 24 samples for which the clast content was accurately determined. This range concurs with the 5 to 30 vol% content established by Vishnevsky and Montanari (1999), but is significantly more restricted than noted by Masaitis *et al.* (1998), who cite clast contents up to 70 vol%. The clasts comprise mineral fragments of quartz, orthopyroxene and plagioclase, with lesser amounts of alkali feldspar, clinopyroxene, biotite, hercynite, lithic igneous and gneissose clasts and glass fragments. Neither the total clast fraction nor the clast composition varies consistently with depth or location in the sampled cores.

Monocrystalline and polycrystalline quartz comprises 9.3 to 91.9% of the clast component (Table 2). Quartz clasts range from unstrained varieties to those displaying sutured subgrain boundaries and a preferred crystallographic alignment of subgrains typical of pre-impact-related tectonic fabrics in the target rocks (Fig. 3a).

Plagioclase clasts comprise 7.7 to 44.1 vol% of the clast population. The majority of the plagioclases are unzoned

TABLE 1. Textural attributes of Popigai melt rocks and their clastic load.

Sample	Clast attributes				Other attributes		
	Maximum diameter (mm)	Average diameter (mm)	± (2σ)	Vol% of rock	Av. gmass grain size (μm)	Max. gmass grain size (μm)	Minimum corona width (μm)
High-temperature (HT) samples							
1-110	5.3	1.0	0.6	24.8	10	20	20
1-338	2.5	0.7	0.9	16.0	29	40	80
2-313	nd	nd	nd	nd	75	100	200
3-140(2)	6.2	0.6	0.3	31.6	7	15	40
3-205.6	3.5	1.0	0.5	25.4	7	10	100
3-350	3.3	0.6	0.3	22.1	19	41	75
3-480	2.2	0.8	0.4	11.3	75	100	200
3-480(2)*	1.3	0.5	0.3	12.6	75	100	200
9-320	2.9	0.7	0.4	16.6	14	24	50
9-340	3.9	0.6	0.2	18.6	15	20	0
13-123	1.7	0.4	0.2	24.4	3.3	10	0
13-286	2.3	0.6	0.3	16.9	22	40	80
Low-temperature (LT) samples							
1-131.5	6.1	0.6	0.3	30.1	7	10	50
1-140	10.5	1.1	0.9	31.9	11.1	20	20
1-178	1.6	0.4	0.2	13.4	3.1	6	0
2-340	nd	nd	nd	nd	12.5	20	40
3-256	1.7	0.6	0.3	12.2	36	50	40
3-305	3.4	0.5	0.4	22.7	19	40	10
3-500	2.4	0.6	0.4	12.2	50	75	100
6-735	2.8	0.7	0.5	11.4	55	100	10
6-780	2.3	0.5	0.3	24.0	9	15	2
9-100	2.2	0.6	0.4	12.5	7	10	0
9-461m1†	2.1	0.5	0.2	30.1	8	12	8
9-461m2†	1.1	0.4	0.4	1.0	9	11	8
13-135	3.5	0.5	0.2	35.5	4	9	8
13-175	4.1	0.8	0.7	25.1	7	14	50

Abbreviations: Av. = average; gmass = groundmass; Max. = maximum; nd = not determined

*Duplicate clast analysis of 3-480 indicates that the data are reproduceable.

†Two melts with contrasting clastic contents in this sample were assessed individually.

TABLE 2. Clast composition of 17 Popigai impact melt rocks.

Sample	Unshocked quartz	Toasted/ PDF quartz	Ballen quartz	Lechat.	Clastic tridymite	Decom-posed clasts*	CPX	OPX	Glass	Melted plag.	Unmelt. plag.	Fine gr. recryst. plag.	Acicular recryst. plag.	Alkali feldspar	Lithic clasts	Opaque†	Other‡
High-temperature (HT) samples																	
1-110	30.1	19.0	1.1	0.0	0.0	20.5	2.9	0.0	5.8	11.6	0.8	0.0	0.0	0.0	0.0	0.6	7.5
1-338	3.6	22.6	0.0	0.0	0.0	19.0	6.7	0.9	3.5	33.7	2.2	0.0	0.0	0.6	0.0	1.2	6.0
3-140(2)	17.3	0.7	0.0	0.0	0.0	0.0	6.8	0.0	30.5	27.9	1.5	0.3	4.6	0.0	10.4	0.0	0.0
3-205.6	37.1	1.5	1.6	0.8	0.0	1.1	0.7	0.0	48.4§	5.4	0.2	0.0	3.3	0.0	0.0	0.0	0.0
3-350	6.1	7.8	0.3	0.0	0.0	28.0	0.0	5.0	18.0	5.9	3.2	2.1	13.7	0.0	0.0	0.8	9.1
3-480	0.8	18.1	5.0	0.0	0.0	34.9	4.1	1.7	1.9	10.3	5.3	0.0	6.8	0.0	3.6	2.7	4.7
3-480(2)#	0.7	8.6	0.0	0.0	2.8	42.7	7.8	3.7	1.0	8.2	6.9	0.0	5.1	0.0	3.2	2.2	7.1
9-320	1.5	8.0	6.6	0.0	0.0	32.8	0.0	1.8	0.2	12.3	6.7	0.0	22.5	0.0	4.4	0.6	2.5
9-340	5.0	16.6	0.4	0.0	25.0	10.1	0.0	2.0	2.8	10.6	4.5	0.0	13.7	0.0	0.6	4.3	4.4
13-286	2.9	9.8	0.0	0.0	0.0	38.9	0.1	5.6	0.6	11.4	13.2	2.9	2.9	0.0	1.6	5.4	4.8
HT mean	10.5	11.3	1.5	0.1	2.8	22.8	2.9	2.1	7.2	13.7	4.5	0.5	7.3	0.1	2.4	1.8	4.6
Low-temperature (LT) samples																	
1-131.5	14.6	2.9	0.0	0.0	0.0	1.9	1.0	0.0	20.4	8.7	0.8	0.0	34.6	0.6	0.0	5.6	9.0
1-140	60.3	2.6	0.0	1.6	0.0	13.3	1.1	0.6	3.6	10.2	2.2	0.0	0.4	0.1	1.1	0.5	2.6
1-178	33.4	5.2	0.0	0.0	0.0	0.2	1.1	0.0	0.6	13.8	9.2	0.0	12.3	0.0	10.1	1.5	12.6
3-500	33.8	0.0	0.0	0.0	7.4	30.2	3.4	0.0	0.0	14.7	0.9	0.0	0.9	0.0	1.4	0.2	7.0
6-735	83.5	8.4	0.0	0.0	0.0	0.0	0.4	0.0	0.0	0.0	0.2	0.0	7.5	0.0	0.0	0.0	0.0
9-100	37.0	0.5	0.0	0.0	0.0	0.8	3.0	2.3	0.0	24.5	7.2	0.0	9.1	0.0	0.0	4.6	11.2
13-175	25.5	6.1	0.0	0.0	0.0	18.4	0.8	2.3	0.3	5.5	1.9	2.9	8.7	0.0	23.3	2.5	1.8
LT mean	41.2	3.7	0.0	0.2	1.1	9.3	1.5	0.7	3.6	11.0	3.2	0.4	10.5	0.1	5.1	2.1	6.3
Overall mean	23.1	8.1	0.9	0.1	2.1	17.2	2.3	1.5	5.6	12.6	3.9	0.5	8.6	0.1	3.5	1.9	5.3

Abbreviations: PDF = planar deformation features; Lechat. = lechatelierite; CPX = clinopyroxene; OPX = enstatite orthopyroxene; Plag. = plagioclase; Fine gr. = fine-grained; Unmelt. = unmelted; recryst. = recrystallized.

*Melt clasts and patchy mesostasis melts are difficult to distinguish in this sample. The total here is an amalgamation of these melt types.

†Includes hercynite spinel.

‡Clasts whose original composition prior to alteration cannot be determined, as well as other uncommon clast types (*e.g.*, biotite).

§Clasts of mono/polycrystalline quartz which have been significantly/totally replaced by glass + OPX.

#Duplicate of 3-480 indicates that although the clast load is reproduceable (Table 1) the relative fraction of clast types can differ substantially.

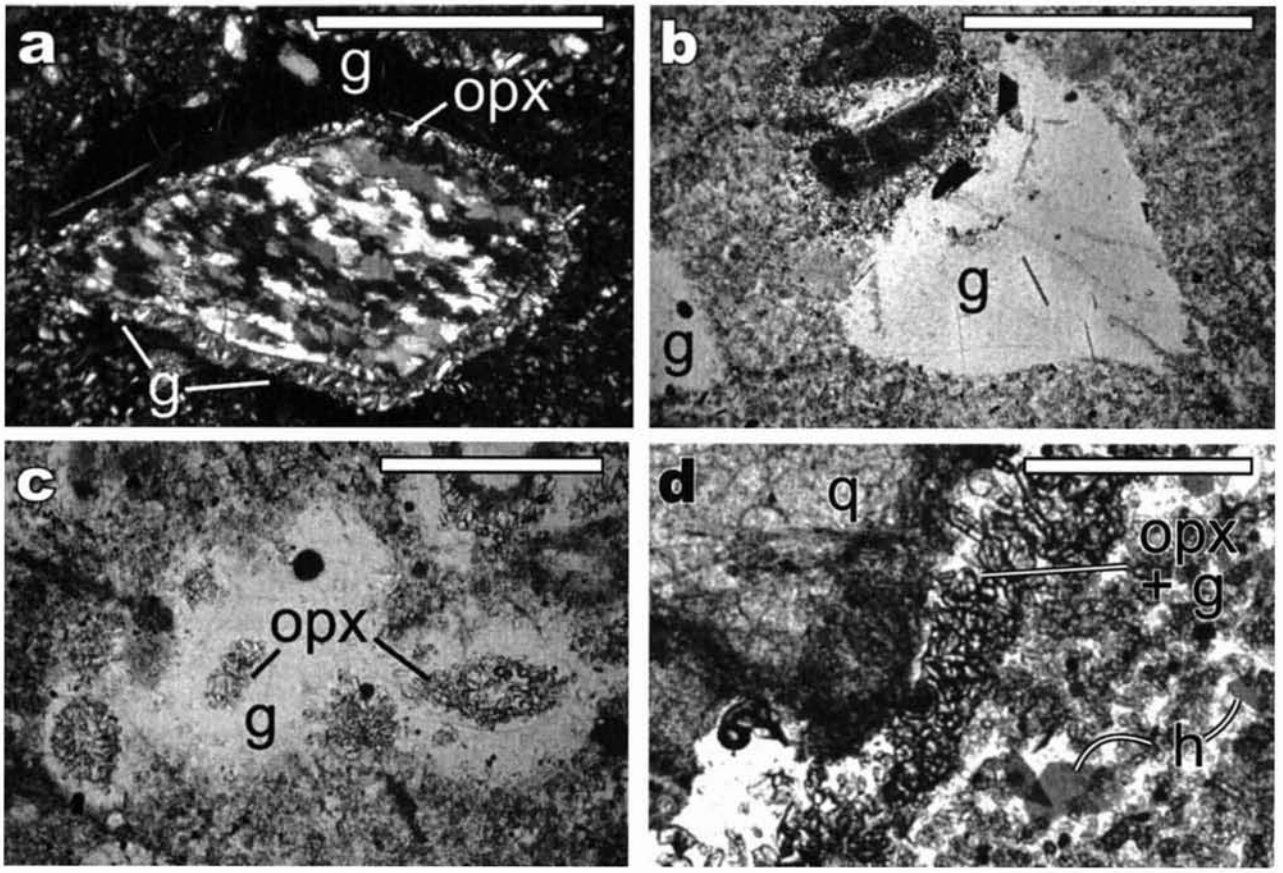

FIG. 3. Photomicrographs of clasts within the impact melt rocks. Scale bars are 0.5 mm long. (a) A quartz clast exhibiting high-strain features preserved from the pre-impact target. Enstatite (opx)–glass (g) coronas are commonly developed on quartz clasts (cross-polarized light; XPL). (b) Typical glass clasts with a sharp, angular contact with the groundmass. Note the acicular ilmenite needle in the larger glass clast and the shocked (toasted) quartz with a well-developed reaction corona near the top of the photograph (plane polarized light; PPL). (c) Variably decomposed quartz clasts, having been replaced with opx and glass (relic quartz is preserved only in the right-hand example, PPL). Note their gradational, irregular margins. (d) A glass–opx reaction corona on a larger quartz clast (q). Subhedral, fractured hercynite spinel clasts (h) are present in the groundmass (PPL).

andesines and labradorites (Fig. 4). Plagioclase clasts display a range of textures, which depend upon their degree of shock and, in some cases, subsequent recrystallisation. These include unmelted and undeformed clasts, partially melted clasts locally exhibiting kinked or bent twinning, recrystallized fine-grained clasts and clasts that comprise randomly oriented fine- to medium-grained acicular or prismatic crystals.

Pyroxene clasts include up to 5.6 vol% enstatite (mean composition $En_{58.5}Fs_{40.3}Wo_{1.2}$), and up to 7.8 vol% diopside-augite (mean composition $Wo_{44.4}En_{41.9}Fs_{13.7}$). Zoning is generally absent in the pyroxene clasts. However, where present in the orthopyroxene, it involves a <3 wt% decrease in SiO_2 and accompanying increase in Al_2O_3 towards the rim, and a 1–2 wt% decrease in the enstatite component towards the rim.

Rounded to angular clasts of clear, pale pink to brown glass locally occur in the melt rocks. These comprise up to 12.3 vol% (*e.g.*, samples 3-205.6 and 9-340) (Fig. 3b). They possess sharp contacts with the surrounding mesostasis of the melt rocks, implying that they were solid or highly viscous when incorporated. Most of the glass clasts are holohyaline, though some contain very fine-grained, irregularly-oriented orthopyroxene needles and/or hercynite crystals in their cores. Patches of glass ± orthopyroxene also occur in the melt rock, where quartz clasts have completely reacted with the surrounding melt. In contrast to these patches of reaction glasses, the glass clasts possess sharp rather than gradational contacts. In addition, where pyroxene needles are present, they occur in the cores of the clasts but not at the margins, as is the case for the reaction glasses (Fig. 3c). Glass clasts can most easily be distinguished from reaction glass patches where the glass clasts retain their original angular morphology (Fig. 3b). The glass clasts can be compositionally indistinguishable from the hosting groundmass mesostasis of the melt rocks.

Minor clastic components include hercynite spinel, biotite, lechatelierite (after quartz), lithic clasts and potassic feldspar. The hercynite spinels are unzoned and have a composition that does not vary more than 0.04 Fe or Mg atomic units from the average of $Fe_{0.61}Mg_{0.40}Cr_{0.01}Al_{1.98}O_4$, which probably represents their original composition in the target rocks. The

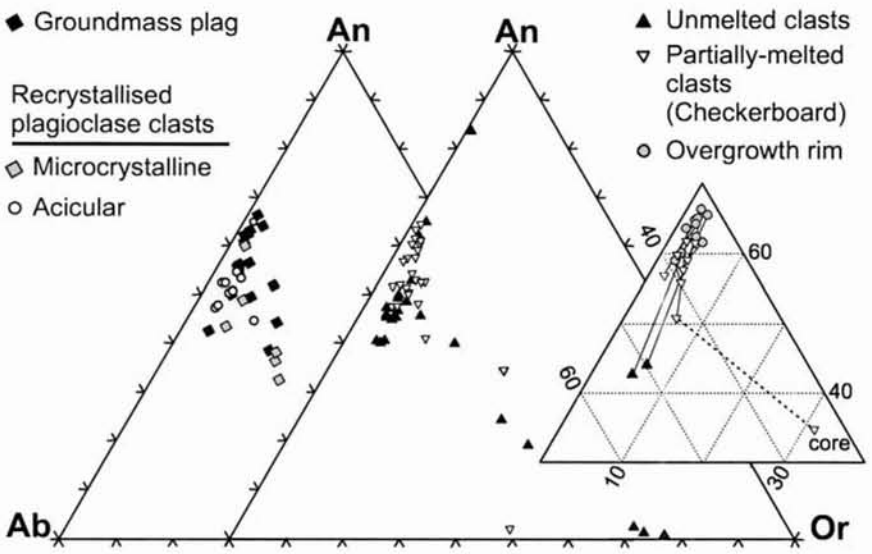

FIG. 4. Anorthite, albite, orthoclase (An, Ab, Or) plots displaying the compositions of plagioclase in the melt groundmass, recrystallized clasts, melted and unmelted plagioclases, and overgrowth rims. The expanded ternary diagram (right) links plagioclase clast rims with Ca-rich overgrowth mantles. The core of one K-rich clast is linked to its low-K rim with a dashed line.

hercynite is commonly fragmented, but occasionally the euhedral-subhedral hexagonal habit of the original crystals is preserved (Fig. 3d). The hercynite displays an unusual strong deep purple color in plane-polarized light, which is more typical of spinel *(sensu stricto)* than hercynite (Deer *et al.*, 1992).

Lithic clasts constitute up to 23.3 vol%, though typically comprise <5 vol% of the clast load (Table 2). Igneous lithic clasts are more common than sedimentary lithic clasts, though this is most probably not indicative of their pre-impact areal extent in the target rocks.

Potassic feldspar clasts comprise <1 vol% of the clast population and contain 36.0 to 76.7% Or, with a mean composition of $An_{10}Ab_{31}Or_{60}$. They are generally recrystallized into very fine-grained, equant crystals. However, the lack of any morphological evidence of flow in the clasts suggest that the potassic feldspars did not fuse. These feldspars are locally mantled by more calcic and less potassic overgrowth rims (mean $An_{42}Ab_{49}Or_9$), that are more potassic than similar overgrowths on the plagioclases.

Clast Melting and Reaction Textures

Reaction between some of the quartz clasts with the surrounding melt has resulted in orthopyroxene + glass coronas (Fig. 3a,c,d). This feature of impact melt rocks occurs in the Mistastin (Grieve, 1975), Manicouagan (Simonds *et al.*, 1978), Chicxulub (Kring and Boynton, 1992), Sääksjärvi and Lappajärvi (Bischoff and Stöffler, 1984) impact structures, among others. In some cases at Popigai, quartz clasts up to 1.5 mm in diameter have been completely replaced by orthopyroxene and glass such that their original textures are obliterated (Fig. 3c). These "decomposed clasts" can comprise up to 43 vol% of the total clast population (Table 2). Pyroxene in the coronas ($En_{55-59}Fs_{40-45}Wo_{0-2}$) is unzoned, possesses a composition that is similar to that of the groundmass pyroxene, and does not vary in composition across the coronas.

It is common for the quartz clasts to be mantled by an inner corona of glass and an outer corona of radially arranged orthopyroxene crystals and intersertal glass (Figs. 3d and 5a). The glass is similar in composition to the groundmass mesostasis and does not vary across the coronas, nor with proximity to the enstatite crystals. An outer corona of fibrous potassic feldspar with crystals that radiate outwards from the clast is only locally present around the glass ± pyroxene coronas (Fig. 5a).

Some of the plagioclase clasts in the Popigai impact melt rocks comprise small subgrains with intervening glass and secondary crystallisation products, which yield a texture elsewhere referred to as "checkerboard feldspar" (Grieve, 1975) (Fig. 5b). These checkerboard feldspars typically possess a uniform ratio of plagioclase to melt glass from core to rim. Each checkerboard element comprises a region of plagioclase that remains in crystallographic continuity with adjacent plagioclase elements, surrounded by melt glass (Fig. 5b).

Both normal and checkerboard plagioclase clasts in a single sample possess indistinguishable compositions ($An_{40-65}Ab_{33-54}Or_{2-20}$ and $An_{35-65}Ab_{34-47}Or_{1-31}$, respectively), indicating that composition is not the factor that controlled the development of the texture (Fig. 4). Although the melt glass in the checkerboard plagioclase possesses a wider range of CaO than do glasses in other textural relationships in the melt rocks (Fig. 6), it is statistically indistinguishable from interstitial glass in the groundmass. The melt glass composition does not vary from the core to the rim of the enclosing checkerboard

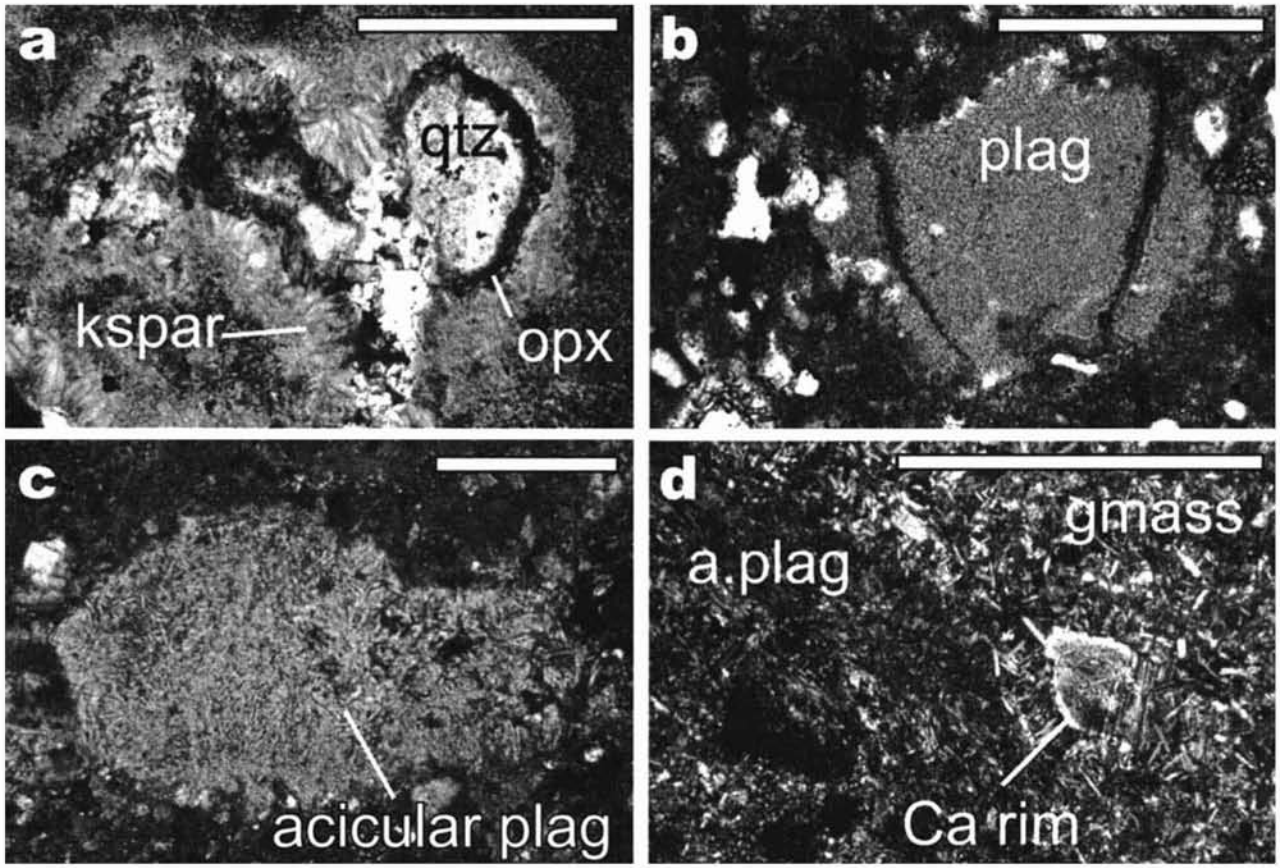

FIG. 5. Photomicrographs of feldspars in the melt rocks. Scale bars represent 0.5 mm. (a) A radiating alkali-feldspar (kspar) corona outside the typical opx–glass corona (PPL). (b) A partially-melted plagioclase clast (plag) with incipient, small-scale "checkerboard" texture (PPL). (c) and (d) Recrystallisation of diaplectic glasses surrounded by groundmass (gmass) results in acicular masses of new plagioclase with no preferred orientation. Note that the Ca-rich overgrowth mantle on the partially melted plagioclase clast in (d) is missing on the right-hand side of the clast owing to breakage of the clast following the mantle development.

plagioclase. Notably, it is also significantly different from a pure plagioclase melt and contains euhedral, igneous crystals of enstatite.

In addition to monocrystalline "checkerboard" plagioclases, microcrystalline plagioclases and those comprising a mesh of irregularly oriented acicular and prismatic plagioclase crystals also occur (Fig. 5c). The polycrystalline plagioclases and checkerboard feldspars possess overlapping compositional ranges ($An_{33-60}Ab_{37-49}Or_{3-23}$ and $An_{45-65}Ab_{33-49}Or_{2-12}$, respectively).

Overgrowth rims of plagioclase are common on checkerboard feldspar clasts that display partial-melting textures, but are typically absent on normal plagioclase grains in the same thin section. The overgrowth rims are up to 20 μm wide and possess a fairly uniform average composition of $An_{63}Ab_{34}Or_2$, which contain from 2.7 to 18.5% more anorthite than the compositionally varied clasts on which they grew (Fig. 7). Overgrowths that have developed on potassic feldspar are significantly less potassic and more calcic than the clast cores. Overgrowth rims on plagioclase clasts have been noted in melt rocks from other impact structures, where they are typically calcic (*e.g.*, Grieve, 1975; Bischoff and Stöffler, 1984), although they can be sodic or potassic (Grieve, 1978; Floran *et al.*, 1978). The overgrowth rims at Popigai bridge and "seal" the melt channels at the margins of the checkerboard plagioclase clasts (Fig. 7).

Locally, enstatite clasts appear texturally similar to checkerboard plagioclases, in that melt (glass) channels can breach adjacent cleavages, resulting in discrete subgrains of pyroxene that maintain their optical continuity (Fig. 8). The spacing between the melt channels tends to be greater than that observed in plagioclase, producing a more crude "checkerboard texture". Checkerboard pyroxene and non-checkerboard pyroxene clasts possess similar compositional ranges (Fig. 9).

Melt glasses within the pyroxenes are similar to those recorded for the groundmass mesostasis glass, demonstrating that these glasses are not simply *in situ* pyroxene melts (Fig. 6). Locally, where spherical, immiscible pyrrhotite droplets are common in the groundmass, they are also found in the melt channels in the pyroxenes (Fig. 8).

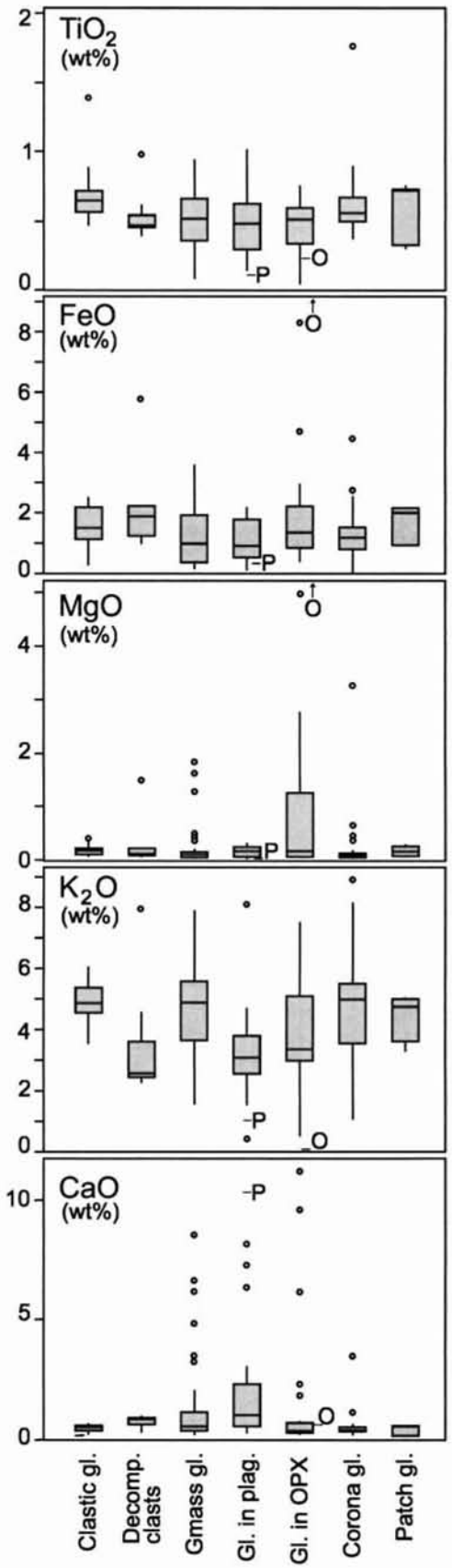

FIG. 6. *(left)* Boxplots showing the range of selected oxide contents of glasses occurring in various textural relationships in the Popigai melt rocks. Boxes define the interquartile range (median values are shown in the boxes as a line), the whiskers extend from the box to a distance of 1.5× the interquartile range, or to the highest actual value within this range. Outliers (circles) are data points that lie outside the range of the maxima and minima of the whiskers. Abbreviations: gl. = glass; Decomp. = decomposed quartz glass; Gmass. = interstitial groundmass glass; Gl. in plag. = glass in checkerboard plagioclases; Gl. in OPX = glass in partially melted orthopyroxene; Corona gl. = glass in reaction coronas around quartz clasts; Patch gl. = irregularly shaped regions of glass in the impact melt rock. The average composition of melting plagioclase and orthopyroxene is shown as P and O, respectively, for comparison with melts found in those minerals. With the exception of the melt clasts, the margins of each of the melt types are gradational.

Reaction coronas similar to those seen on quartz are not present on the enstatite clasts, though they are locally present on augite. The pyroxenes in the coronas on the augite clasts have a composition that is statistically indistinguishable from those on quartz clasts ($En_{57-60}\,Fs_{37-42}Wo_{1-4}$) (Fig. 9).

Melt Rock Subtypes and Interrelated Characteristics

We have performed two sample *t* tests on the clast content, average and maximum clast size, average and maximum groundmass grain size and the minimum reaction corona width data for 22 melt rocks. We have made these statistical comparisons to assess whether the subdivision of the melt rocks supplied and previously subdivided into HT and LT groups by the Karpinsky Geological Institute, Russia, accurately separates subgroups that possess similar textural characteristics. These statistical tests evaluate whether the means calculated for the HT and LT populations are significantly different. The results indicate that HT and LT samples do not differ significantly in terms of their mean clast contents, clast sizes or groundmass grain sizes (Table 3). There is, however, a statistically significant difference in the corona widths in samples visually divided into HT and LT groupings, though the *t* test demonstrates that this difference is not large. The range of values for all the above characteristics measured in the HT samples do not differ significantly from the range of the LT samples.

We have evaluated the degree of correlation between the measured textural features. There is a good correlation between higher clast volumes and the lower average groundmass grain sizes (correlation factor, C.F. of −0.775, where values approaching 1 and −1 represent excellent correlations, and zero values represent no correlation) (Fig. 10). This supports similar observations for impact melt rocks from the Manicouagan, Lappajärvi and Chicxulub impact structures (Floran *et al.*, 1978; Reimold, 1982; Claeys *et al.*, 1998, respectively). There is also a good correlation between the minimum width of the reaction coronas around quartz and the average groundmass grain size (C.F. of 0.808), and a weak correlation between the volume percentage clasts and the corona width (C.F. of −0.495). Other characteristics display poorer correlations (Fig. 10).

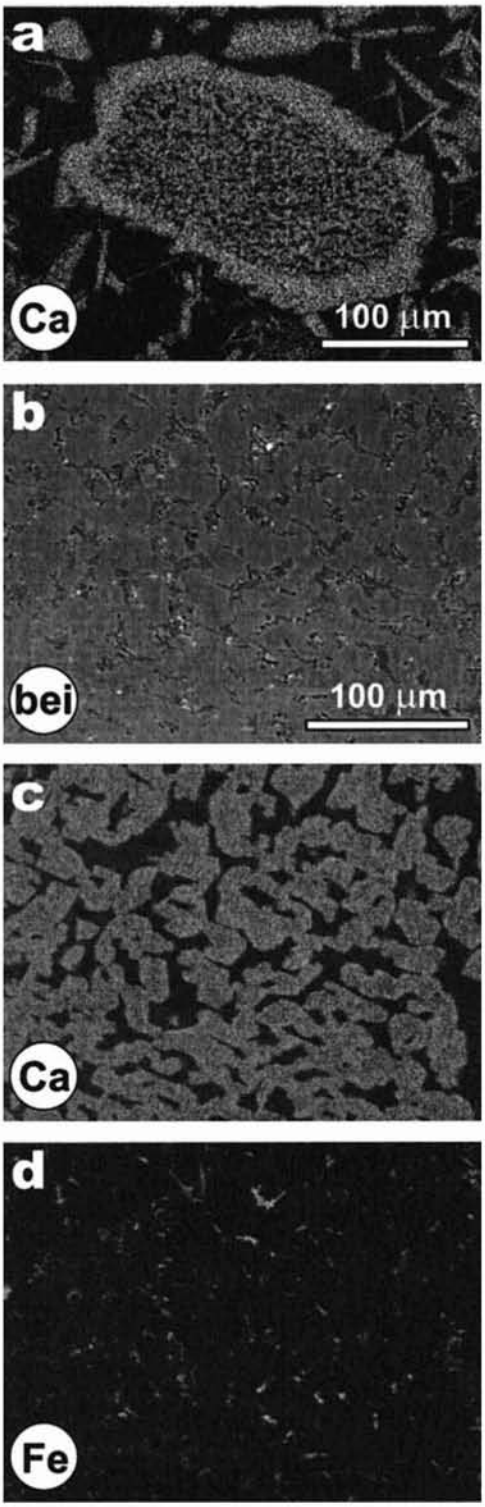

FIG. 7. A partially melted plagioclase clast. (a) Ca x-ray compositional map showing a contiguous Ca overgrowth rim sealing a porous, partially melted core. (b) A backscattered electron image, (c) Ca, and (d) Fe x-ray compositional maps, respectively, of the same region of a "checkerboard" plagioclase. (c) The relic plagioclase subgrains (light grey tone) surrounded by glass (dark tone) are subhedral, owing to secondary plagioclase growth following the melting process. (d) The presence of fine-grained pyroxene is defined by areas with a higher Fe content (lighter grey tone).

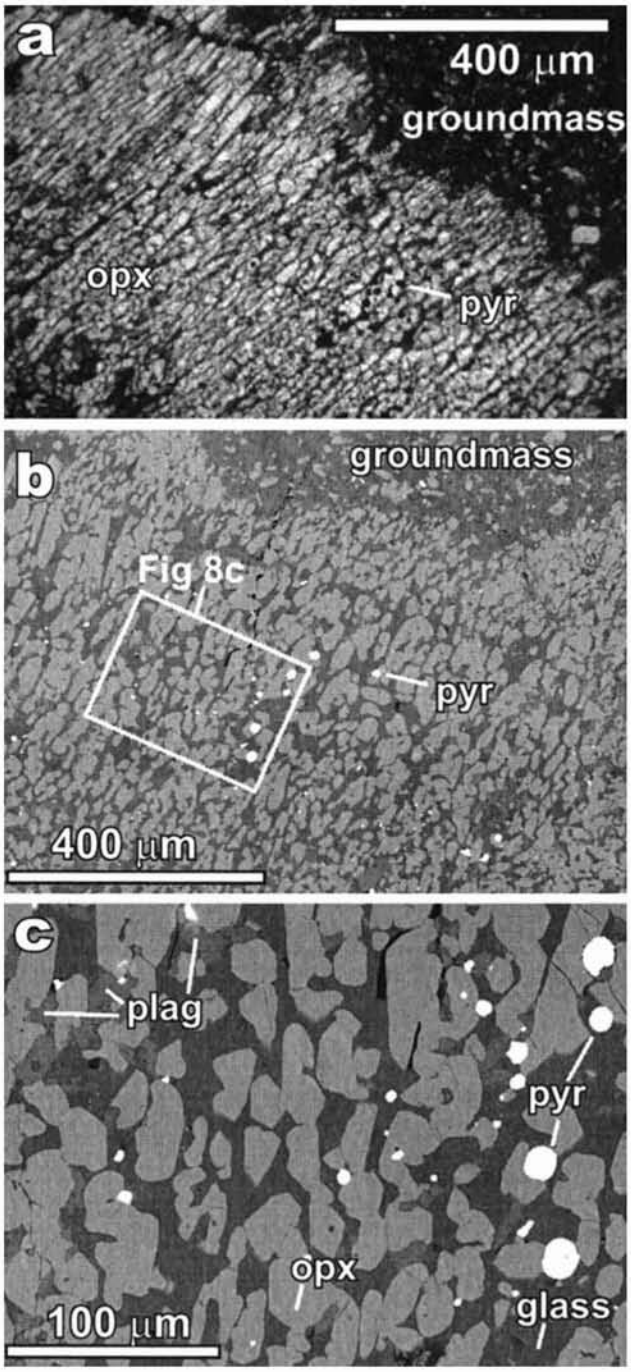

FIG. 8. A partially melted enstatite clast. (a) Photomicrograph showing the whole of the pyroxene in optical (and therefore crystallographic) continuity, despite the presence of melt between the pyroxene subgrains. This suggests that the pyroxene subgrains remain connected in three-dimensions and have not been rotated with respect to one another (XPL). Immiscible globules of pyrrhotite (pyr) that are also present in the lower secondary electron images are labeled. (b) and (c) Backscattered electron images. The new growth of pyroxene on the skeletal, remnant pyroxene is responsible for the subhedral habit and the partial overgrowth of the pyrrhotite globules. Secondary interstitial growth of plagioclase (plag) is evident.

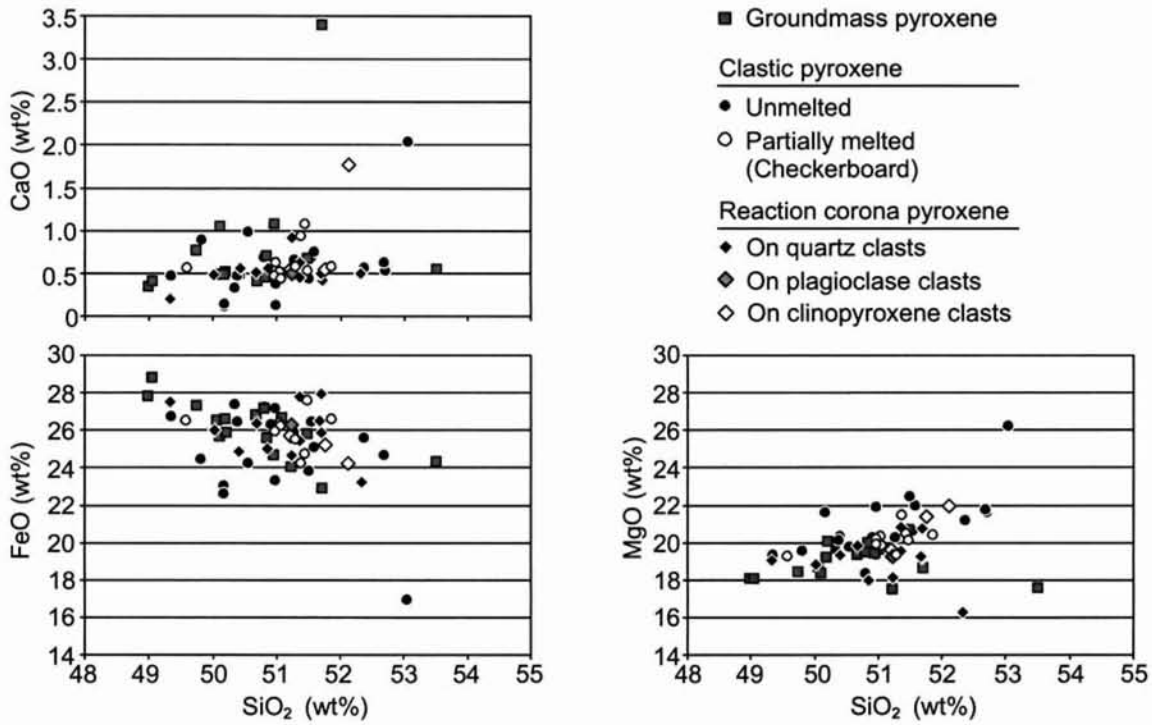

FIG. 9. The composition of groundmass, clastic and reaction corona pyroxenes in the melt rocks.

TABLE 3. *t* test results.

Characteristic	$t_{calculated}$
Clast fraction (%)	0.46
Mean clast size	0.57
Max. clast size	0.38
Mean gmass g. size	0.60
Max. gmass g. size	0.49
Min. corona width	2.38

Tests performed using 11 high-temperature and 11 low-temperature randomly chosen samples. $t_{critical} = 2.09$, based on a *df* value of 20 ($n = 22$), for a level of significance of 0.05. Values of $t_{calculated} < 2.09$ indicate that no significant difference exists between the high-temperature and low-temperature populations for these criteria.
Abbreviations: Max. = maximum; Min. = minimum; gmass = groundmass; g. size = grain size.

SHOCK FEATURES

Shock features present in the melt rocks at Popigai and observed as part of this study are summarized in Fig. 11. These range from unshocked clasts and deformation features that are not uniquely indicative of impact, such as kinking of biotite clasts, through the full range of shock levels including bulk rock melting (*i.e.*, shock pressures >60 GPa) and mineral vaporization (as demonstrated by the locally vesiculated plagioclase melt clasts). Other workers have noted the presence of coesite and stishovite at Popigai (Vishnevskii *et al.*, 1974; Vishnevsky *et al.*, 1975), though these minerals do not extend the shock pressure range beyond that which is defined by the other shock features noted as part of this study.

Target rocks that have not been melted and homogenized with the bulk impact melt rocks are preserved as clasts that exhibit an array of shock metamorphic features in single thin sections. It is not uncommon to find shear-attenuated schlieren of lechatelierite (>50 GPa; Grieve *et al.*, 1996) alongside unshocked clasts in the melt rocks, indicating that turbulent flow within the melt rocks has mixed clasts that have experienced vastly different shock conditions.

Shocked quartz at Popigai is commonly brownish with a grainy texture in both plane- and cross-polarized light. This coloration is common in many other impact structures (Whitehead *et al.*, 2002), and has been referred to elsewhere as "toasted quartz" (Short and Gold, 1996) (Fig. 12a). Single and multiple PDFs are best developed in those grains exhibiting toasting. Individual grains can display the toasted texture unevenly, with no preferential distribution at the rims or cores, or at grain asperities. Toasted regions coincide with areas of preferential PDF development, consistent with there being a shock component to the origin of the toasted regions. No major element compositional heterogeneity was revealed by high-power backscattered electron imaging or x-ray compositional mapping. No difference in backscattered grey scale was noted. Transmission electron microscope (TEM) studies indicate that there are large quantities of 50–80 nm void space in the toasted quartzes, that were probably filled

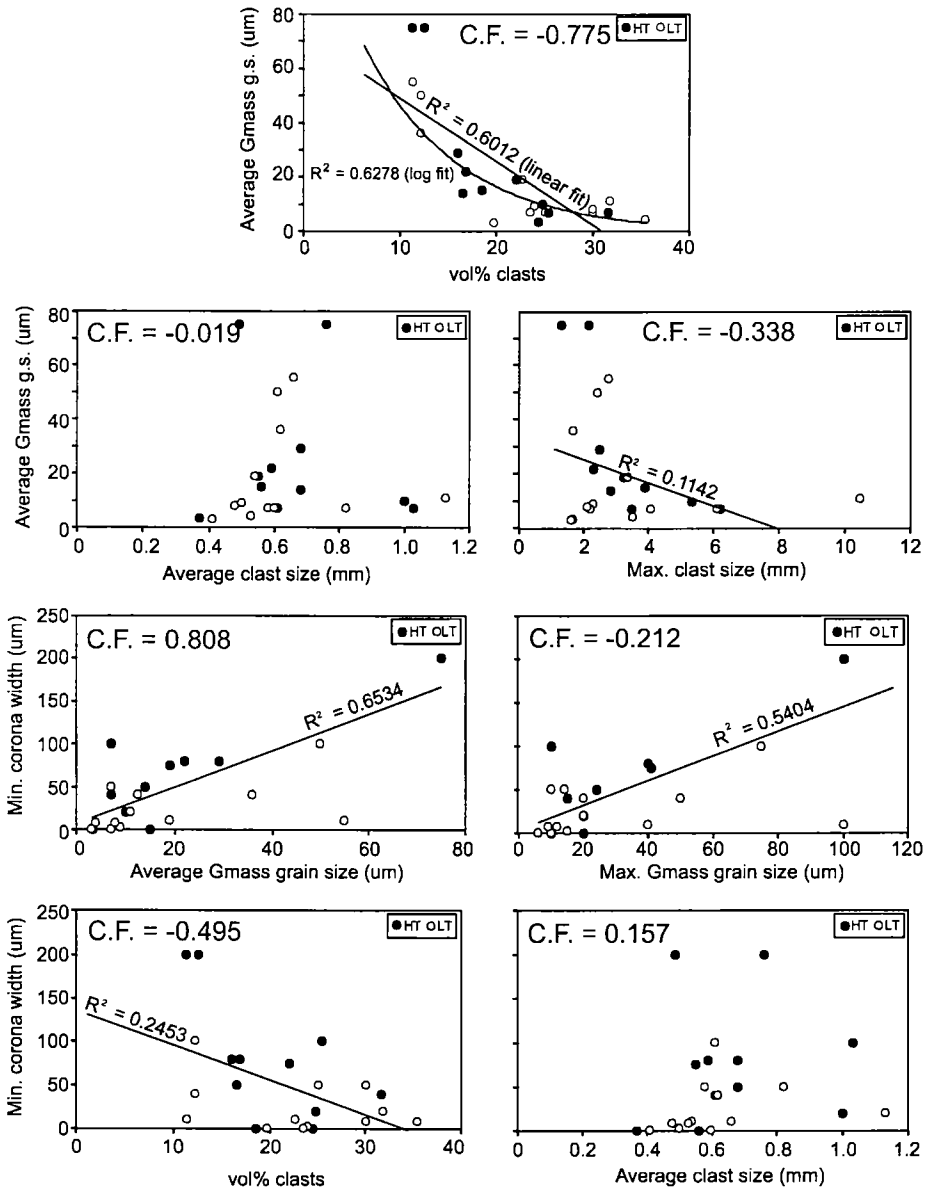

FIG. 10. Comparison of clast and groundmass attributes. So-called high-temperature (HT) and low-temperature (LT) melt rocks display no consistent differences. The degree of fit to the trend lines (R^2) and the correlation factor (C.F.) are shown. Grain size (g.s.) refers to the groundmass (Gmass) grain size.

with gas or fluid, and which are related to the toasted texture. The results of these studies, and the probable origin of this coloration, are presented in a separate contribution (Whitehead *et al.*, 2002).

Quartz containing arcuate fractures that form a fish-scale pattern, known as ballen quartz (von Engelhardt, 1972), is commonly present (Fig. 12b). The concave side of the fractures typically face toward the centre of the clasts, though it is not uncommon for them to face in the opposite direction. The ballen are present in both toasted and untoasted quartz. Ballen have been interpreted to develop in response to the 7% volume shrinkage that accompanies the high–low inversion of cristobalite, prior to its transformation to quartz at lower temperatures (von Engelhardt, 1972). The presence of relic metastable cristobalite was originally inferred from refractive index studies of Fennoscandian ballen (Carstens, 1975). This has since been confirmed using Raman spectroscopy on ballen from the Wanapitei impact structure, Canada (Polsky and McHone, 1998). We isolated mono- and poly-mineralic felsic phases with densities <2.5 g/cm^3 from several ballen quartz-bearing Popigai melt rocks using heavy liquids, and analysed these using x-ray diffraction techniques. The results reveal the presence of α-cristobalite belonging to the $P42_12_12$ space group, which confirms the space group identified by Raman spectroscopy. α-tridymite was also identified by XRD analysis.

All three types of ballen present in impact melt rocks, as described from the Lappajärvi impact structure (Bischoff and

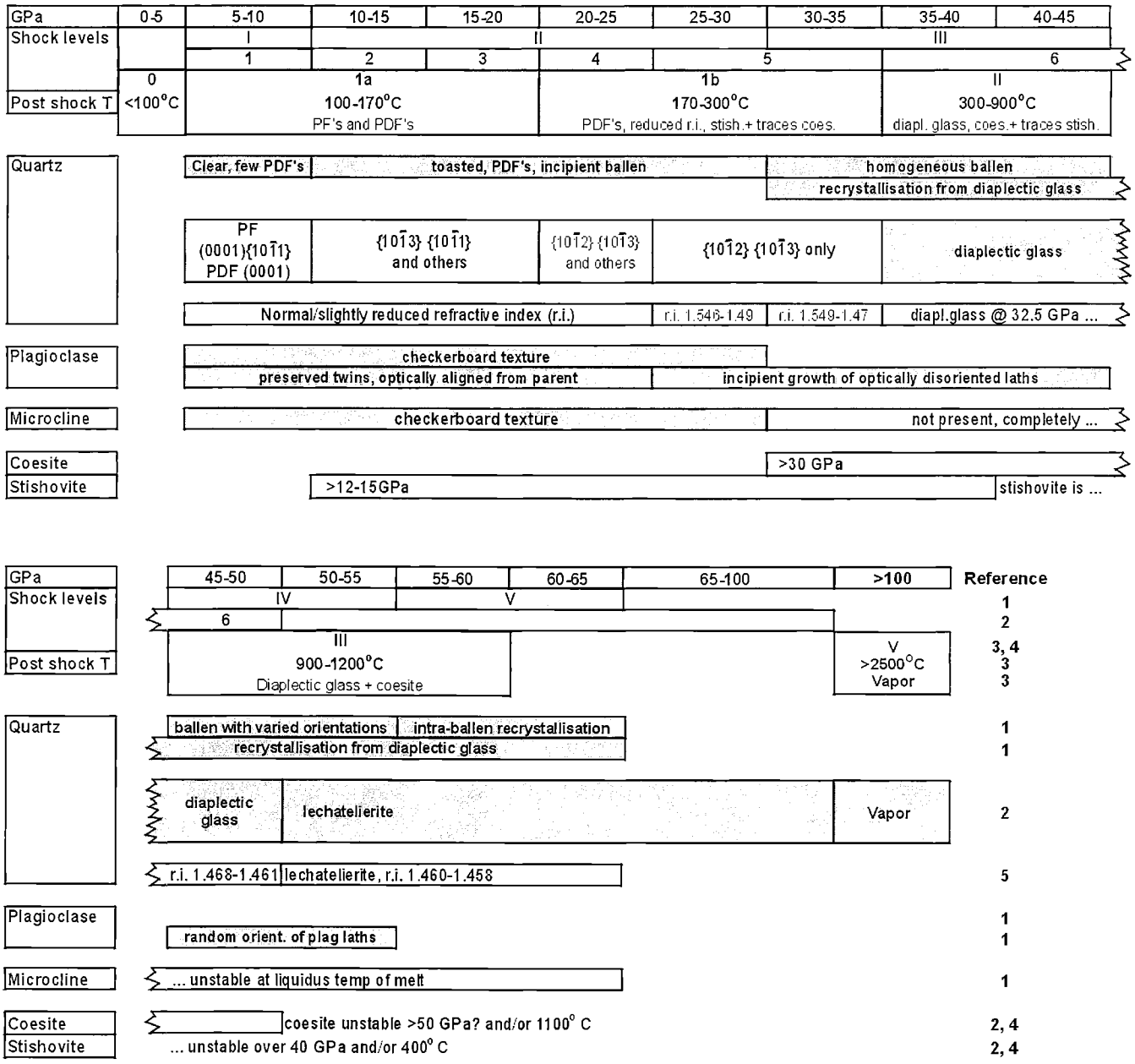

FIG. 11. A compilation of shock metamorphic features observed in impact melt rocks. Those features in grey boxes were encountered during this study. Note that equal numerical values on different shock level scales do not necessarily refer to equivalent shock features. These scales are only to be used for non-porous, crystalline rocks (Grieve *et al.*, 1996). Abbreviations: r.i. = refractive index; stish. = stishovite; coes. = coesite; diapl. = diaplectic. References: (1) Bischoff and Stöffler (1984); (2) Grieve *et al.* (1996); (3) Stöffler (1984); (4) Stöffler and Langenhorst (1994); (5) Langenhorst and Deutsch (1994).

Stöffler, 1984), are present in the Popigai melt rocks. These comprise (1) ballen with a uniform crystallographic orientation across the clast; (2) individual ballen that possess distinct extinction orientations from neighbouring ballen; and (3) clasts in which the ballen have been uniformly overprinted by small, polygonal crystals with discrete crystallographic orientations. These correspond to shock levels III (30–45 GPa) to V (55–65 GPa), respectively, of Bischoff and Stöffler (1984).

GEOCHEMISTRY

Major and Trace Element Data

Bulk impact melt rocks sampled from the widest range of crater-radial, crater-concentric and depths possible from the sampled cores were chosen for major element (25 samples) and trace element (37 samples) analysis. On the basis of texture and

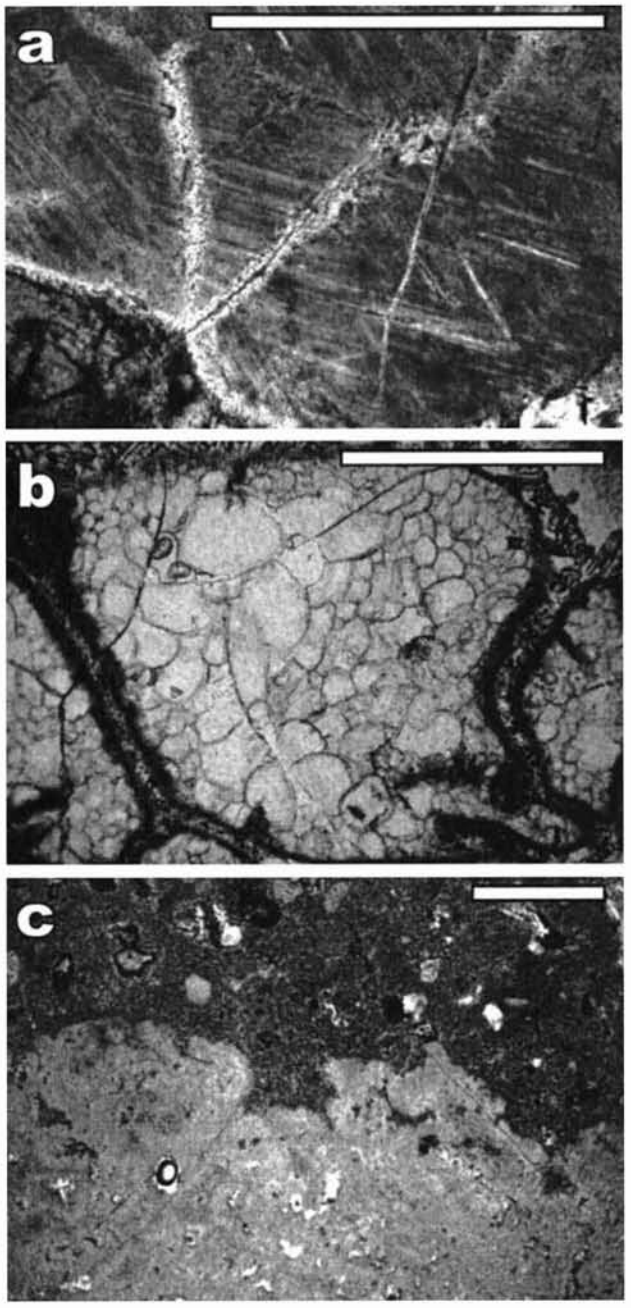

FIG. 12. Photomicrographs of shock metamorphic features and intermixed melt rocks. Scale bars are 0.5 mm long. (a) Multiple sets of planar deformation features observed in "toasted" quartz (PPL). (b) Ballen quartz (PPL). (c) Two texturally discrete melt rocks with a nebulous contact indicative of incipient intermixing at high temperatures (PPL).

major element contents, the melt rocks are classified as high-K andesites and rhyolites (60.7 to 67.9 wt% SiO_2). The presence of normative corundum indicates that they are peraluminous.

The samples possess a limited range of major and trace element compositions (Tables 4 and 5). Several of the lower concentration oxides (TiO_2, MnO, Na_2O, P_2O_5 and CO_2) vary less than analytical uncertainty.

The major element compositions of the HT and LT melt rocks were compared statistically using univariate (ANOVA) and multivariate (MANOVA) analyses of variance. Although previous studies have found that the two groups display different SiO_2 contents (Masaitis *et al.*, 1998), the application of these statistical tests to the 25 new major element data found no significant differences between the two groups. Similarly, no difference was found between the trace element contents, nor the H_2O, CO_2, F and Cl contents of the HT and LT melt rocks.

The impact melt rocks possess major element contents similar to those of gneisses in the target (Table 4). The ϵNd and ϵSr isotopic signatures of the melt rocks also fall within the range of three target gneiss samples of Hölker *et al.* (1997), which is consistent with the melts having been derived by fusion of the gneisses, though the isotopic compositions of other potential source rocks in the target have yet to be determined.

While it must be borne in mind that the sampled melt rocks are not part of a single coherent melt sheet, we have evaluated the distribution of the trace elements in the melt bodies to assess whether compositional trends are present in the study area. We determined the C.F. for the concentration of the trace elements as a function of (1) depth in the cores, and (2) radial distance from the crater centre. The mean C.F. value, when considering concentration in relation to depth, was only 0.16 ± 0.12, while the highest factors of only 0.31 to 0.36 are attributable to weak increases of Sn, Cr, Ni and Mo with depth and a weak decrease of Cs with depth (C.F. –0.36). Eighty-six percent of the C.F. values for concentration *vs.* radial distance were <0.3, with a mean value of 0.18 ± 0.15. Values that exceed 0.3 include Sb (0.57), Pb (0.47), Sn (0.39), Cl (–0.37) and Nb (–0.39), though the significance of such low correlation factors is questionable. These low values are not surprising given the lack of compositional variation in the melt rocks. In summary, the data indicate that the impact melt rocks are fairly homogeneous in three dimensions in the study area.

Projectile Considerations

The average Ni, Cr and Co contents of the 37 melt rocks are shown in Table 6. The Ni and Co values are within the range of values reported in Masaitis and Raikhlin (1986), though we find significantly higher Cr contents (Table 6). The melt rock concentrations are higher than mean values in the target gneisses. This has been attributed to the contamination of the melt rocks by the projectile (Masaitis and Raikhlin, 1986). Low concentrations of Ni in achondrites, and low Cr contents in iron meteorites (Mittlefehldt *et al.*, 1998) preclude these meteorite types as probable impactors since they could not produce the observed siderophile element enrichment in the melt rock. After correcting for the indigenous fraction of these siderophile elements from the target gneisses, the Ni/Cr, Cr/Co and Ni/Co ratios should be those of the impacting body.

Two values for the indigenous components were presented in Masaitis and Raikhlin (1986): those for the average of 41

TABLE 4. Major element compositions of melt rocks and the mean target gneiss.

Core/depth (m)	SiO_2	TiO_2	Al_2O_3	Fe_2O_3*	MnO	MgO	CaO	Na_2O	K_2O	P_2O_5	H_2O	CO_2	LOI	Total
1/1	64.20	0.74	14.10	7.21	0.08	3.99	4.18	2.40	2.40	0.13	1.4	0.3	nd	100.7
2/144-154	66.10	0.65	13.50	7.06	0.07	2.83	3.39	2.10	2.56	0.10	2.4	0.5	nd	100.8
2/144-154(2)	66.20	0.67	13.50	6.97	0.07	2.85	3.42	2.10	2.55	0.10	2.3	0.5	nd	100.9
2/180.5	62.40	0.76	14.10	7.21	0.07	3.74	4.26	2.00	2.88	0.12	2.6	0.3	nd	100.3
2/323	67.90	0.82	13.00	6.66	0.05	2.35	1.34	2.50	2.42	0.07	2.9	0.7	nd	100.4
3/325-335	62.90	0.74	14.20	7.92	0.07	3.67	4.23	2.30	2.78	0.12	1.6	0.7	nd	100.8
3/450	63.40	0.74	14.20	7.32	0.07	3.59	3.69	2.30	2.78	0.12	2.8	0.3	nd	100.9
3/530	63.80	0.74	14.60	7.18	0.07	3.61	4.03	2.40	2.79	0.12	1.5	0.2	nd	100.8
6/64-69	61.90	0.74	14.70	7.70	0.07	3.71	3.95	2.20	2.84	0.11	2.3	0.5	nd	100.5
6/115-120	63.60	0.73	14.20	7.88	0.08	3.62	3.81	2.30	2.72	0.12	1.8	0.2	nd	100.6
6/262-267	63.00	0.73	14.40	7.52	0.07	3.45	3.82	2.30	2.95	0.12	2.0	0.5	nd	100.6
6/334-339	63.20	0.72	14.20	7.82	0.07	3.45	3.76	2.30	2.66	0.12	2.3	0.4	nd	100.7
6/349-354	64.00	0.73	13.90	7.37	0.07	3.23	3.65	2.30	2.78	0.11	2.1	0.4	nd	100.5
6/544-549	63.30	0.74	14.40	7.86	0.07	3.41	3.89	2.30	2.83	0.12	1.8	0.4	nd	100.9
6/763-768	62.40	0.77	14.10	7.57	0.07	3.75	4.12	2.40	2.75	0.14	2.6	0.4	nd	100.8
9/75	62.80	0.75	14.00	7.15	0.07	4.21	5.05	2.20	2.83	0.14	1.1	0.3	nd	100.4
9/160	63.30	0.74	14.30	7.17	0.07	3.61	3.97	2.30	2.79	0.12	1.7	0.4	nd	100.3
9/270	63.10	0.75	14.40	6.98	0.07	3.80	4.52	2.30	2.81	0.12	1.3	0.4	nd	100.3
9/300	63.20	0.74	14.40	7.55	0.07	3.56	3.93	2.30	2.95	0.12	1.4	0.5	nd	100.6
9/430	63.60	0.75	14.50	7.20	0.07	3.60	4.05	2.30	2.79	0.12	1.4	0.4	nd	100.6
12/97	62.50	0.75	14.00	8.29	0.08	3.47	3.81	2.20	2.56	0.12	2.4	0.5	nd	100.2
12/147.9	62.80	0.71	14.30	7.10	0.07	3.40	3.34	2.20	2.84	0.10	3.0	0.3	nd	99.9
13/93	63.10	0.72	14.30	7.33	0.08	3.59	3.78	2.30	2.55	0.12	2.6	0.2	nd	100.4
13/220	60.70	0.69	13.90	nd	0.08	3.43	3.47	2.18	2.55	0.10	nd	nd	3.1	99.3
13/300	62.30	0.69	13.90	nd	0.08	3.52	3.87	2.18	2.69	0.11	nd	nd	1.6	99.2
Average	63.43	0.73	14.12	7.39	0.07	3.50	3.81	2.27	2.72	0.12	2.1	0.4	2.4	100.5
1σ st. dev.	1.47	0.03	0.37	0.38	0.01	0.38	0.63	0.11	0.15	0.01	0.6	0.1	1.1	0.4
Target gneiss composition (Masaitis *et al.*, 1998)														
Mean (n = 45)	63.44	0.77	15.47	7.67	0.07	3.20	3.00	2.57	2.47	0.09	1.65	nd	nd	99.81
1σ st. dev.	2.69	0.16	1.45	1.51	0.03	0.69	1.00	0.48	0.86	0.07	0.97	nd	nd	nd

Abbreviations: LOI = loss on ignition; st. dev. = standard deviation; nd = not determined.
Sample 2/144-154(2) is a duplicate analysis of sample 2/144-154.
*Total iron is reported as Fe_2O_3.

TABLE 5. Trace element compositions of Popigai melt rocks (excluding REE).

Core/depth (m)	Cr	Ni	Co	Sc	V	Cu	Pb	Zn	Sn	Mo	S	Sb	Ag	Rb
1/1	131	51	18	15	96	35	15	71	0.0	1.1	1326	0	0.0	99
2/144-154	131	63	15	13	85	54	23	68	5.9	2.1	983	2.1	0.0	77
2/144-154(2)	128	63	16	13	84	59	23	68	4.3	2.7	nd	2	0.0	75
2/180.5	145	62	21	16	100	39	16	82	0.9	1.4	1470	0	1.4	82
2/323	157	38	15	13	102	15	39	79	0.6	0.0	314	2.3	0.0	71
3/188-198	145	57	17	15	102	46	23	80	12.0	1.8	1558	2.1	0.0	78
3/325-335	140	63	18	15	98	56	24	82	4.3	2.9	1447	2.3	0.0	86
3/450	154	58	18	16	101	41	17	86	1.0	1.6	1716	0.3	1.5	85
3/530	146	55	16	16	101	38	22	78	2.6	1.3	1528	1.2	0.4	86
6/115-120	143	56	19	15	101	43	30	84	5.1	1.2	1522	3.4	0.0	84
6/246-251	146	62	17	15	101	58	24	85	5.0	2.6	1548	2.5	0.0	84
6/262-267	138	53	17	15	101	42	18	84	3.1	1.3	1370	0.6	0.0	89
6/334-339	139	56	17	15	97	44	21	83	3.0	1.9	1416	1.4	0.0	80
6/349-354	132	56	16	14	94	51	20	75	2.8	1.9	2077	1	0.0	86
6/400-405	155	68	18	16	105	61	21	84	3.5	2.9	1683	1.1	0.0	87
6/513-518	151	67	18	15	103	59	16	100	4.6	3.0	1495	0.6	0.0	88
6/544-549	141	65	17	15	99	58	17	82	2.4	3.0	1317	0.5	0.0	87
6/64-69	133	58	18	16	96	52	23	87	4.0	1.6	1707	1.9	0.0	82
6/688-693	152	97	19	14	96	101	51	86	18.0	7.0	1608	1.2	0.0	79
6/763-768	138	70	16	14	96	55	18	88	2.9	3.0	942	0.8	0.0	93
7/328.2	131	59	17	15	97	112	15	112	1.2	2.5	1229	0	0.0	85
7/402.9	143	71	19	15	99	95	15	94	1.4	3.6	1600	0.2	0.0	83
7/91.3	134	64	19	15	98	190	16	161	1.3	3.0	1244	0	0.0	90
9/160	134	53	18	16	101	36	17	82	1.1	1.4	1371	0.3	0.0	86
9/270	130	50	18	15	98	34	17	77	1.3	1.0	1167	0.4	0.0	85
9/300	137	57	17	16	103	53	15	80	9.0	1.4	1738	0	0.0	90
9/430	133	52	18	16	102	36	18	80	1.5	1.0	1547	0.5	0.0	86
9/75	126	49	16	15	98	33	17	77	1.3	1.4	903	0.5	0.0	89
11/281	155	87	21	15	99	74	14	70	2.2	4.5	1960	0.3	0.0	90
11/304	149	77	19	14	109	66	14	75	1.0	7.0	3929	0	0.0	84
11/340	144	68	19	15	98	56	15	72	1.4	3.2	2014	0.2	0.0	86
11/93.9	147	74	18	15	98	62	14	71	1.3	3.0	1106	0.4	0.0	88
12/147.9	153	64	17	16	99	42	15	80	0.0	1.7	1985	0	0.4	83
12/97	143	68	18	16	103	58	15	73	1.2	3.0	1848	0	0.0	68
13/220	147	67	19	16	101	59	15	81	1.7	2.9	2079	0.3	0.0	87
13/300	138	62	17	15	97	53	17	74	1.9	2.5	1931	0.4	0.0	87
13/93	136	52	17	16	102	40	14	77	0.6	1.2	1630	0	0	110
Average	141	62	18	15	99	57	20	83	3.1	2.4	1564	0.8	0.1	85
1σ st. dev.	9	11	1	1	5	29	7	16	3.5	1.4	548	0.9	0.3	7

Core/depth (m)	Cs	Sr	Tl	Ga	Ta	Nb	Hf	Zr	Y	Th	U	F	Cl	Be
1/1	1.40	214	0.43	17	0.6	13	6.1	236	34	14	1.8	721	131	1.2
2/144-154	0.80	236	0.37	16	0.6	11	5.9	236	30	11	1.4	570	225	0.9
2/144-154(2)	0.83	243	0.36	16	0.6	11	6.3	252	30	11	1.4	nd	nd	nd
2/180.5	0.81	235	0.48	17	0.7	14	6.6	261	35	13	1.7	770	194	1.0
2/323	0.38	182	0.20	15	0.6	13	8.3	331	35	8.5	1.4	295	0	nd
3/188-198	0.85	218	0.39	16	0.5	11	6.5	258	34	13	1.7	731	219	0.8
3/325-335	0.71	225	0.47	18	0.6	12	6.5	257	33	14	1.9	830	146	1.0
3/450	0.78	232	0.44	17	0.6	13	6.4	256	35	13	1.7	782	184	0.9
3/530	0.63	236	0.44	17	0.6	13	6.3	248	35	14	1.7	890	124	0.8
6/115-120	0.80	231	0.44	18	0.6	12	6.9	283	34	15	1.7	764	157	1.0
6/246-251	0.74	225	0.46	17	0.6	12	6.3	255	34	14	1.8	801	150	1.0
6/262-267	0.75	225	0.49	17	0.6	12	7.0	276	35	14	2.5	770	172	1.0

TABLE 5. *Continued.*

Core/depth (m)	Cs	Sr	Tl	Ga	Ta	Nb	Hf	Zr	Y	Th	U	F	Cl	Be
6/334-339	0.65	217	0.41	17	0.6	12	6.0	244	33	12	1.6	723	108	1.1
6/349-354	0.64	217	0.45	17	0.6	12	6.1	243	33	13	1.7	758	0	1.0
6/400-405	1.80	224	0.40	17	0.6	12	6.3	253	35	14	1.8	698	109	1.0
6/513-518	0.89	227	0.41	18	0.6	12	6.4	250	35	13	1.7	816	234	1.1
6/544-549	0.64	228	0.43	17	0.6	13	6.5	254	35	14	1.7	847	117	1.0
6/64-69	0.89	220	0.45	18	0.6	12	6.1	241	36	14	2.0	986	0	1.0
6/688-693	0.58	222	0.43	17	0.6	12	6.6	259	34	14	2.3	782	214	1.0
6/763-768	0.78	203	0.51	18	0.6	12	6.5	260	31	17	1.7	870	0	1.2
7/328.2	1.10	236	0.46	17	0.6	12	6.3	243	34	13	2.1	766	208	1.1
7/402.9	0.61	222	0.44	17	0.6	12	6.2	238	35	14	1.7	886	126	1.1
7/91.3	1.40	241	0.41	17	0.6	12	6.2	245	33	13	1.9	727	160	1.1
9/160	0.85	220	0.47	17	0.6	12	6.2	247	34	14	1.7	779	201	0.9
9/270	0.91	238	0.46	17	0.7	13	6.2	244	33	14	1.7	808	270	1.0
9/300	0.79	219	0.49	17	0.7	13	6.3	248	35	14	1.6	912	429	0.9
9/430	0.61	230	0.45	18	0.6	13	6.7	271	36	14	1.7	886	138	0.9
9/75	0.85	242	0.48	17	0.6	13	6.4	245	34	14	1.9	634	330	1.1
11/281	0.96	217	0.44	17	0.6	12	6.4	252	34	16	1.7	651	156	0.7
11/304	0.79	218	0.38	17	0.6	12	6.4	252	33	15	1.6	758	195	0.9
11/340	0.78	227	0.47	17	0.6	13	6.5	250	36	15	1.8	704	177	0.9
11/93.9	0.74	219	0.41	17	0.6	12	6.2	248	34	15	1.7	819	104	1.0
12/147.9	0.85	207	0.44	17	0.5	12	6.0	240	34	12	1.5	813	157	0.8
12/97	1.10	235	0.36	17	0.7	13	6.6	258	35	13	1.7	684	137	0.9
13/220	0.78	216	0.43	17	0.6	13	6.3	249	36	14	1.7	758	196	0.9
13/300	0.82	220	0.45	17	0.6	15	6.4	258	35	15	1.8	817	184	1.1
13/93	1.3	225	0.29	17	0.62	13	6.3	256	36	14	1.7	681	181	1
Average	0.85	224	0.43	17	0.6	12	6.4	254	34	14	1.7	764	162	1.0
1σ st. dev.	0.26	12	0.06	1	0.0	1	0.4	17	1	1	0.2	116	86	0.1

Abbreviations: st. dev. = standard deviation; nd = not determined.
Cd, In and Te concentrations were generally close to or below detection limits and are not presented.
Sample 2/144-154(2) is a duplicate analysis of sample 2/144-154.

TABLE 6. Siderophile element composition of the Popigai rocks.

	Masaitis and Raikhlin (1986)		This study	
	Unshocked gneiss	Average gneiss	Unshocked gneiss	Average gneiss
Gneiss*				
Ni, Cr, Co (ppm)	13, 22, 11	27, 80, 13	13, 22, 11	27, 80, 13
Tagamites†				
Ni, Cr, Co (ppm)	85 ± 31, 110 ± 18, 19 ± 4	85 ± 31, 110 ± 18, 19 ± 4	62 ± 11, 141 ± 9, 18 ± 1	62 ± 11, 141 ± 9, 18 ± 1
Meteoritic‡				
Ni, Cr, Co (ppm)	72 ± 31, 88 ± 18, 8 ± 4	58 ± 31, 30 ± 18, 6 ± 4	49 ± 11, 119 ± 9, 7 ± 1	35 ± 11, 61 ± 9, 5 ± 1
Ni/Cr§	0.8 ± 1.7	1.9 ± 1.7	0.4 ± 1.2	0.6 ± 1.2
Ni/Co§	9.0 ± 7.8	9.7 ± 7.8	7.4 ± 11.0	7.5 ± 11.0
Cr/Co	11.0 ± 4.5	5.0 ± 4.5	17.9 ± 9.0	13.2 ± 9.0

*Masaitis and Raikhlin (1986) analysed 18 unshocked gneisses and 41 gneisses in total (shocked and unshocked).
†Masaitis and Raikhlin (1986) report 85, 83, and 79 analyses for Ni, Co and Cr, respectively. We report the mean of 37 analyses.
‡The meteoritic component is the difference between the tagamite and gneiss values.
§The meteoritic ratios calculated using the unshocked gneiss correction reported in Masaitis and Raikhlin (1986) were erroneously calculated and are correctly presented here.
All errors are 1σ.

shocked and unshocked gneisses; and those for 18 unshocked gneisses alone. The Ni/Cr, Ni/Co and Cr/Co meteorite ratios, which they claim to be most similar to L chondrite values, were erroneously calculated based on an amalgam of correction values: a Ni value from the unshocked gneisses and Cr and Co correction values from the average gneisses. We present the recalculated meteorite ratios based on the melt rock measurements of Masaitis and Raikhlin (1986) and our new data using both the mean gneiss corrections and the unshocked gneiss corrections (Table 6 and Fig. 13). None of the calculated sets of meteorite ratios are similar to those of any of the chondritic meteorite types, and an L-type chondrite cannot be inferred from current data. Vishnevsky and Montanari (1999) assessed the possible contribution of Ni, Cr, Co and Ir from mafic and rare ultramafic rocks that are locally present in the target. They concluded that while the Ir in the melt rocks could also have an ultramafic target provenance, the anomalously high concentrations of this element likely have a meteoritic source; albeit, heterogeneously distributed. Consequently, a contribution of Ni, Cr and Co from the ultramafic lithologies is considered minimal. However, the heterogeneity of the target gneiss siderophile contents preclude a unique indigenous correction. This, coupled with the heterogeneous siderophile contents of the melt rocks, can explain the difficulty that has been experienced in assigning the inferred meteoritic siderophile components to those of known chondrite types.

Rare Earth Element Data

The rare earth element (REE) concentrations of the 37 melt rocks analysed possess a uniform pattern (Table 7; Fig. 14) with significant light (L)REE enrichment (mean La_N/Sm_N of 4.55) and slight heavy (H)REE depletion (mean Gd_N/Yb_N of 1.42). The LREE, in particular, exhibit a range of concentrations (*e.g.*, La_N from 117 to 161), though varied inter-element ratios between samples imply that this variability is not a result of simple fractionation. The melt rocks possess a negative Eu anomaly (mean Eu/Eu* of 0.68).

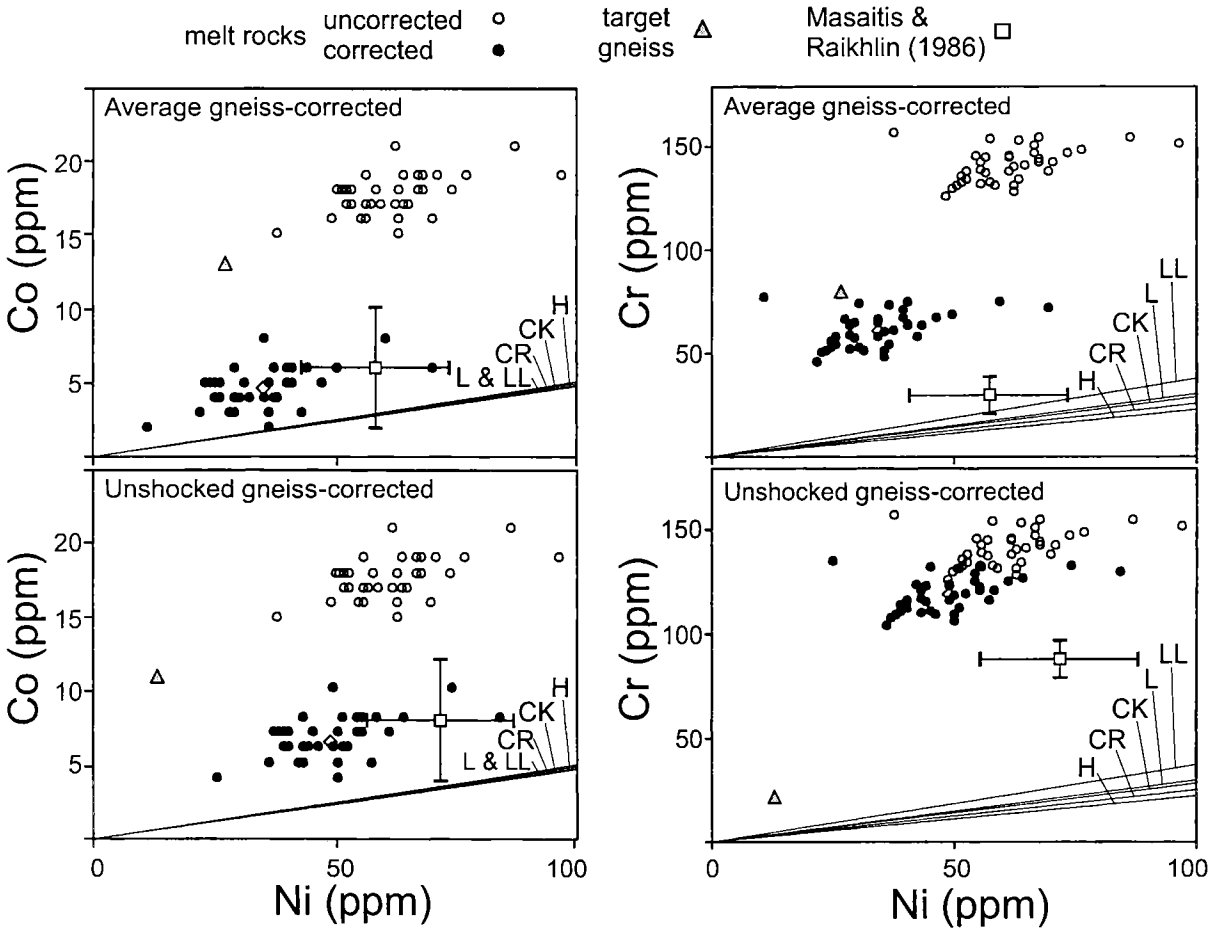

FIG. 13. Ni, Cr and Co contents of 37 Popigai melt rocks ($n = 37$) and the same data corrected for the mean indigenous siderophile contribution from target gneisses (uppermost plots). The lower plots show the melt rock data after correcting for the siderophile contents of 18 unshocked gneisses. The gneiss data is from Masaitis and Raikhlin (1986). The mean corrected melt rock value of these authors is also shown for comparison. The ratios expected in L, LL and H ordinary chondrites and CR and CK carbonaceous chondrites (Kallemeyn *et al.*, 1989, 1991, 1994) possess no similarities with our corrected data or those of Masaitis and Raikhlin (1986).

TABLE 7. REE compositions of Popigai melt rocks.

Core/depth (m)	La	Ce	Pr	Nd	Sm	Eu	Gd	Tb	Dy	Ho	Er	Tm	Yb	Lu
1/1	54	110	13	46	7.4	1.4	5.7	0.88	5.3	1.1	3.0	0.48	3.3	0.48
2/144-154	48	94	11	39	6.2	1.4	4.9	0.76	4.6	1.0	2.6	0.41	2.9	0.43
2/144-154(2)	46	94	11	38	6.3	1.3	5.1	0.78	4.6	1.0	2.6	0.43	3.0	0.44
2/180.5	52	110	12	45	7.3	1.4	5.9	0.89	5.3	1.1	3.0	0.47	3.3	0.50
2/323	43	87	10	37	6.2	1.4	5.4	0.86	5.1	1.1	3.0	0.48	3.3	0.50
3/325-335	54	110	13	45	7.3	1.4	5.8	0.89	5.2	1.1	2.9	0.46	3.2	0.47
3/450	53	110	12	45	7.3	1.5	5.9	0.91	5.5	1.1	3.2	0.50	3.4	0.50
3/530	55	110	13	46	7.6	1.5	6.1	0.94	5.5	1.1	3.2	0.50	3.5	0.52
6/64-69	55	110	13	46	7.6	1.5	5.8	0.93	5.5	1.1	3.2	0.52	3.6	0.52
6/115-120	58	120	14	48	7.5	1.4	5.8	0.87	5.3	1.1	3.0	0.49	3.4	0.49
6/262-267	53	110	13	45	7.4	1.4	5.8	0.88	5.3	1.1	3.0	0.48	3.3	0.50
6/334-339	50	100	12	43	6.9	1.4	5.6	0.85	5.1	1.1	2.9	0.46	3.2	0.47
6/349-354	53	110	12	44	7.1	1.4	5.4	0.85	5.1	1.0	2.9	0.46	3.2	0.47
6/544-549	56	110	13	46	7.4	1.5	5.9	0.90	5.4	1.1	3.1	0.49	3.4	0.49
6/763-768	59	120	14	51	8.1	1.4	5.7	0.83	4.8	1.0	2.7	0.43	3.0	0.45
9/75	53	110	13	46	7.4	1.4	5.8	0.88	5.3	1.1	2.9	0.47	3.2	0.47
9/160	55	110	13	47	7.4	1.5	6.0	0.89	5.4	1.1	3.1	0.49	3.4	0.50
9/270	54	110	13	46	7.5	1.5	5.9	0.90	5.3	1.1	3.0	0.47	3.2	0.48
9/300	54	110	13	46	7.4	1.5	6.1	0.94	5.5	1.1	3.2	0.51	3.5	0.52
9/430	57	110	13	48	7.7	1.5	6.0	0.96	5.6	1.2	3.2	0.50	3.4	0.52
12/97	54	110	13	45	7.6	1.5	6.1	0.94	5.5	1.2	3.2	0.51	3.4	0.51
12/147.9	48	98	11	42	7.0	1.4	5.8	0.89	5.4	1.1	3.1	0.49	3.4	0.51
13/93	53	110	12	45	7.4	1.5	6.0	0.95	5.6	1.1	3.2	0.52	3.5	0.53
13/220	53	110	12	45	7.3	1.5	5.9	0.91	5.5	1.2	3.2	0.50	3.5	0.52
13/300	56	110	13	48	7.5	1.4	5.9	0.90	5.4	1.1	3.1	0.49	3.3	0.50
Maximum	59	120	14	51	8.1	1.5	6.1	0.96	5.6	1.2	3.2	0.52	3.6	0.53
Minimum	43	87	10	37	6.2	1.3	4.9	0.76	4.6	1.0	2.6	0.41	2.9	0.43
Average	53	108	12	45	7.3	1.4	5.8	0.89	5.3	1.1	3.0	0.48	3.3	0.49
1σ st.dev.	4	8	1	3	0.5	0.1	0.3	0.05	0.3	0.1	0.2	0.03	0.2	0.03

Abbreviations: st.dev. = standard deviation.
Sample 2/144-154(2) is a duplicate analysis of sample 2/144-154.

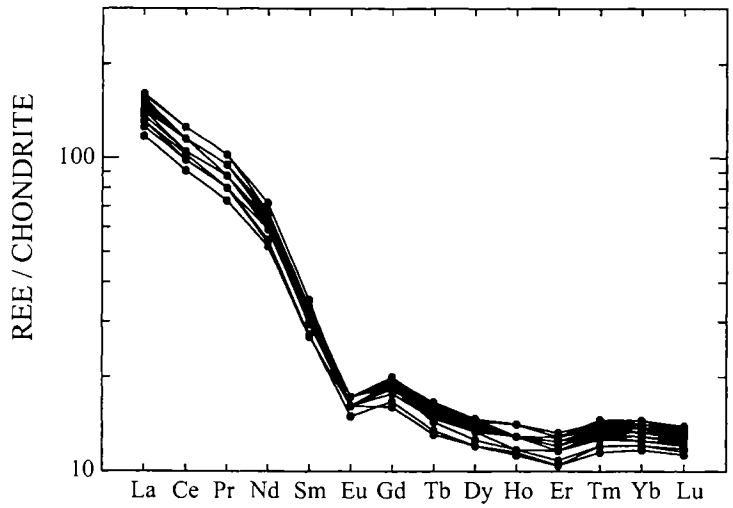

FIG. 14. The rare earth element (REE) patterns of 25 Popigai melt rock samples, normalized to the chondrite values of Taylor and McLennan (1985).

Samarium, Neodymium, Rubidium and Strontium Isotope Data

A composite sample of glass clasts, and a composite sample of felsic clasts were separated from the melt rocks in order to determine their Sm, Nd, Rb and Sr isotopic compositions and ratios. The glass clasts must have been fused and solidified prior to their incorporation in the bulk melt in which they occur, consequently their composition may reflect that of the earliest target rocks melted on impact. These and the felsic clasts were also analysed in order to establish whether they could represent *in situ* analogues to ejected felsic microkrystites deposited in late Eocene marine sediment (Whitehead *et al.*, 2000). The results indicate that although the ϵNd and ϵSr signatures are not identical to those of the homogeneous melt rocks, like the melt rocks, they plot within the range of the isotopically diverse target gneisses from which they too could have been derived (Fig. 15) (Whitehead *et al.*, 2000). The glass clast sample possesses a T(CHUR)Nd model age similar to that of the melt rocks, but a T(UR)Sr model age that is significantly younger. This low T(UR)Sr model age requires Rb-Sr mobilization at a time very much younger than the age of the parental target material, possibly by diagenetic processes. The T(CHUR)Nd model age of the felsic clast sample suggests that this clast may have been derived from target rocks significantly younger than the Proterozoic rocks that formed the melt. The T(UR)Sr model age is only marginally lower than the melt rocks. Analyses of glass coating gneiss bombs ejected from Popigai (Kettrup *et al.*, 2001) (Fig. 15) also plot within the ϵNd and ϵSr values of the target gneisses and exhibit a range of lowered T(UR)Sr ages.

Volatile Element Data

The H_2O, CO_2, Cl and F contents of the bulk melt rock samples presented in Tables 4 and 5 average 2.06 ± 0.56 and 0.40 ± 0.14 wt% oxide, and 158 ± 101 and 765 ± 136 ppm, respectively. The carbon content is significantly higher in the interstitial and patchy mesostasis melts in some samples than in others. The carbon content is not consistently higher in any one type of melt (*e.g.*, reaction melt, mesostasis melt or melt clasts).

DISCUSSION AND CONCLUSIONS

The observations made as part of this study augment previous descriptions of the Popigai impact structure (Masaitis, 1994; Masaitis *et al.*, 1998; Vishnevsky and Montanari, 1999) and can be used to help refine the interpreted history of the impact melt rocks.

Evidence for rapid cooling of the impact melt is manifold. Highly strained quartz clasts display no strain recovery features, such as subgrain boundary migration or polygonization. This indicates that annealing by the enclosing melt was minimal.

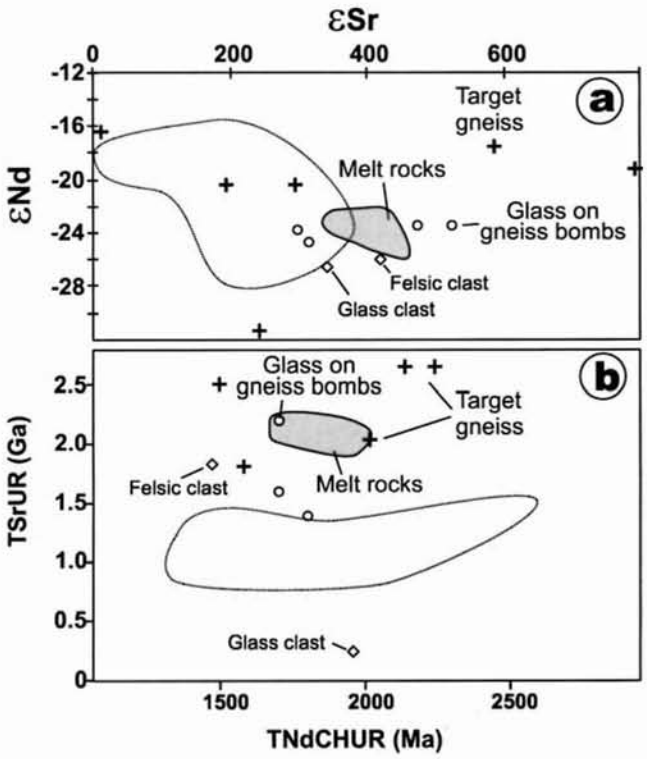

FIG. 15. Nd and Sr isotopic compositions of Popigai melt rocks, basement gneisses (and ejected gneiss bombs), melt coatings on ejecta bombs and a felsic and glass fraction from the melt rocks (data from Stecher *et al.*, 1989; Hölker *et al.*, 1997, Whitehead *et al.*, 2000 and Kettrup *et al.*, 2001). The dotted fields represent the range of late Eocene impact ejecta, inferred to have a Popigai provenance (Whitehead *et al.*, 2000).

Alkali felspar trichites in the most glassy samples are typical of significantly supercooled melts in which the rate of diffusion of atoms necessary for the crystallisation of feldspar was exceeded by their rate of growth (Keith and Padden, 1963). The lack of consistent zoning patterns among the pyroxene clasts implies that their compositions are inherited from the target and that little chemical exchange occurred with the enclosing melt. In addition, rapid cooling of the melt is probably responsible for the preservation of cordierite at the expense of its lower temperature breakdown products, andalusite, quartz and chlorite (Deer *et al.*, 1992). Finally, the lack of evidence of fractionation of the major, trace (including rare earth) elements in the melt rocks also supports rapid cooling.

Melt Rock Subgroups, Grain Sizes and Clast Contents

The melt rocks have previously been subdivided into two groups on the basis of the lustre of hand-samples as it relates to their glass contents (the HT group has a vitreous lustre, the LT group has a non-vitreous lustre; Masaitis, 1994; Masaitis *et al.*, 1998; Masaitis, pers. comm., 2000) (Table 8). Others have defined subgroups based on groundmass grain size (T1 and T2 groups; Vishnevsky and Montanari, 1999). The

TABLE 8. A compilation of the two existing subdivisions of Popigai melt rocks.

	"High temperature" (HT)* or T2†	"Low temperature" (LT)* or T1†
Grain size	Fine grained*/Microcrystalline (10–200 μm)†	Cryptocrystalline* (<10 μm)†
Crystallinity*	Abundant interstitial glass	Holocrystalline
Clast content*	Low (10–35%)	High (60–70% max)
Coronas on quartz*†	Wide (<200 μm)†	Narrow
Loss on ignition	2–3%*, 2.71%†	0.8–1.5% at 250 °C*, mean 1.97%† (montmorillonite clay alteration)
Magnetism	"Natural remanent magnetisation, I_n" is lower by 1–2° magnitude than LT	Higher I_n than HT
Oxidation state	Higher Fe^{2+}/Fe^{3+} than LT* (5.26†)	Lower Fe^{2+}/Fe^{3+} than HT* (3.44†)

*Masaitis (1994); Masaitis *et al.* (1998).
†Vishnevsky (1996); Vishnevsky and Montanari (1999).

different textures have been attributed, by these researchers, to contrasting initial melt temperatures, or contrasting water contents, respectively. We favor the subdivision based on groundmass grain size, since this lends itself to more accurate and consistent quantification. In addition, the proportion of glass may not indicate accurately the initial temperature of the melt. Some of the glasses are generated by reaction with the clasts, some by bulk solidification of the melt rock, and others are clastic glasses. There are also a large number of samples that are not easily assigned to one group or the other based on glass content. For example, some of the coarser-grained samples also contain significant interstitial glass, and thus exhibit a sub-vitreous lustre. It is also curious to note that although it has been stated that the HT melt rocks "are relatively enriched in fresh glass and usually contain less microcrystals in their matrix and less mineral clasts" relative to LT melt rocks (Masaitis, 1994), subsequent reports have revealed that the LT melt rocks can contain 70–90% glass (Masaitis *et al.*, 1998). While our statistical data indicate thicker reaction coronas occur in the HT group, consistent with the observation of Masaitis *et al.* (1998), this is not unexpected because thicker glass-orthopyroxene coronas would result in a more vitreous lustre to the rock in general.

Despite our finding that the samples subdivided into HT and LT groups show no significant difference in terms of the measured characteristics, it is not true to state that the melt rocks are texturally uniform. There are clearly interdigitating melt rocks that can be distinguished on the basis of contrasting groundmass grain sizes, crystallinity or clast content (Fig. 12c). However, our statistical study indicates that the visual hand sample subdivision on the basis of lustre, on which the primary subdivision into LT and HT groupings was made, does not predictably correlate with other characteristics such as actual grain size or clast content.

It has been suggested that the water content of the melt rocks determines whether they crystallized into cryptocrystalline or microcrystalline varieties (Vishnevsky, 1996; Vishnevsky and Montanari, 1999). The heterogeneous distribution of water can better explain the contrasting crystal sizes in intimately intermixed melt rocks than differences in their initial temperatures, because temperature contrasts would be equilibrated rapidly on the small scales observed. Higher water contents can extend the crystallisation period such that larger groundmass crystals have time to develop. However, the relatively thin impact melts in the Manicouagan impact structure are typically coarser grained than those at Popigai, though their water contents overlap within error (1.73 ± 0.37 wt% and 2.1 ± 0.6 wt%, respectively). This suggests that the water content may not have been the sole factor, nor necessarily the principal control, on the final grain size of these impact melts.

Direct cooling of the melt can occur by entraining a significant fraction of cooler clasts in the melt. These clasts can generate chilled margins in the surrounding groundmass, as has been noted around clasts in the Chicxulub impact melt rocks (Warren *et al.*, 1996). However, if they developed, chilled margins are not preserved in the Popigai impact melt rocks. Cooling of the melt bodies might also be expected at their contacts with comparatively cooler suevites. However, sample 4-550 (Fig. 2), while possessing the highest glass content of all the samples studied, is not located near the margin of the melt rock body, where rapid chilling could explain its texture. Indeed, melt rocks sampled within 20–27 m of this sample are significantly more crystalline. This suggests that either the initial temperature of the melts was highly heterogeneous, or that the extent of crystallisation was predominantly dependent on factors other than simply temperature.

A complementary process that could also promote rapid crystallization in a melt, and which is not commonly considered, is the rapid nucleation of groundmass phases on heterogeneously disseminated pulverized clasts. The correlation of higher clast contents with lower grain sizes supports this proposition.

It should be borne in mind that the measured clast contents may not reflect the original clast content because many of the smallest clasts initially present in the melt would have been assimilated. The abundant quartz clasts that remain in the Popigai melt rock commonly exhibit decomposition textures

indicating that they reacted with the surrounding melt and became partially assimilated. The fine-grained texture of the melt rocks, which can reach total thicknesses approaching 800 m (780 m in core 4674), is anomalous when compared with impact melt rocks from other impact structures. For example, the grain size is significantly smaller than that developed in substantially thinner melt rock units from the >80 m thick Mistastin melt sheet (Grieve, 1975) and the >230 m thick Manicouagan melt sheet (Grieve and Floran, 1978). The presence of finely shattered target rock clasts, which may or may not be reflected in the present clast content, could have facilitated rapid, widespread nucleation and consequent limited growth of crystals within the Popigai impact melt rocks. If the Mistastin and Manicouagan impact melts contained a lower concentration of these pulverized clasts then their crystal nucleation rates would not have been accelerated to the same degree as those at Popigai, resulting in their coarser grain sizes. However, in view of the similar basement-sedimentary target rocks at the identically sized Popigai and Manicouagan impact structures, the reason behind the difference in clast content is not immediately apparent.

Most of the clasts in the melt rocks are either mineral clasts of undefinable provenance, or are clearly lithic igneous or metamorphic clasts. There is a significantly low sedimentary rock clast fraction, with a particular lack of carbonate clasts, despite their comprising ~2000 km^3 of the pre-impact target as inferred from the extrapolation of perimeter lithologies beneath the structure. A clastic composition disproportionate to that present in the target has been noted in the impact melt rocks at the Mistastin impact structure, Labrador and on the Moon (McCormick *et al.*, 1989; Spudis *et al.*, 1991). The types of clasts present at Mistastin indicate that the clast lithologies were incorporated during radial melt flow outwards from the region of target fusion, and do not merely reflect the rock types present in the zone of melting. Presumably, radial flow of impact melt at Popigai did not intersect significant near-surface sedimentary rocks. Alternatively, sedimentary clasts, in particular the carbonate rocks, were preferentially melted.

Angular glass clasts probably represent those melts that were formed and quenched in the early stages of crater formation. Isotope data indicate that these glasses do not possess a composition identical to the homogenized bulk melt rock (Whitehead *et al.*, 2000). However, their isotopic character is still consistent with a Proterozoic target gneiss source; albeit a localized one. Although many of these early formed glasses may have been ejected to form local or distal melt ejecta (Whitehead *et al.*, 2000; Kettrup *et al.*, 2001), some were trapped in the chaotic mix of clasts and became incorporated into the mixed melt rocks. Some of the clasts preserve sharp, angular contacts with the surrounding mesostasis, indicating that they were solid when incorporated in the melt rock. Local glass globules probably represent glass clasts that were remelted by heat from the enclosing melt. Turbulent mixing of the melt rocks would have homogenized these glasses with the groundmass glass. Consequently, these clasts are only preserved in those regions of the melt that experienced a comparatively limited period of turbulence.

Clast Coronas

The presence of an inner augite corona and an outer feldspar-bearing corona in the Manicouagan melt rocks led Simonds *et al.* (1978) to suggest that these coronas developed progressively. The limited occurrence of the alkali feldspar coronas at Popigai suggests that either the Popigai melt rocks crystallized more rapidly than those at Manicouagan, thereby restricting the development of these coronas, or that the melt composition did not favour alkali feldspar growth.

X-ray compositional mapping indicates that alkali feldspar is not common in the groundmass of the impact melt rocks. The K_2O content of Popigai melt rocks (Table 4) is also marginally lower than the content in the Manicouagan melt rocks (Floran *et al.*, 1978). These observations, coupled with the absence of outer alkali feldspar coronas on even intensely resorbed quartz clasts at Popigai, suggest that compositional constraints are likely to have restricted the alkali feldspar corona growth in the melt rocks.

In volcanic rocks, glass, clinopyroxene and outer plagioclase reaction coronas have been observed where assimilated quartz xenocryts have reacted with the surrounding enclosing mafic melts (Sato, 1975; McBirney, 1979). It has been proposed that these coronas develop around quartz because the enclosing melt was undersaturated with respect to SiO_2, and consequently the quartz dissolved (McBirney, 1979). The melting of quartz adds SiO_2 to the melt and, as a result, the new melt composition leaves the liquidus and moves into the all liquid field. Thus, the melt corona remains liquid until the melt cools to the point that it again intersects the liquidus. However, the corona glasses around xenocrystic quartz in the Popigai impact melts do not possess a higher SiO_2 content than typical groundmass glasses, which suggests that the addition of silica is not the cause of the coronas. A lack of SiO_2 enrichment in the coronas was also observed in impact melts from the Mien structure (Carstens, 1975). The origin of the coronas remains elusive.

Checkerboard Textures

In a study of rocks from the Lappajärvi impact structure, Finland, checkerboard feldspar was interpreted as having been produced by the total fusion of the plagioclase clasts followed by fractional crystallisation of the melt (Bischoff and Stöffler, 1984). This crystallisation produced strongly zoned subgrains, which are mantled by sanidine and enclosed within a mesostasis of sanidine and quartz.

To explain the crystallographic continuity of each of the newly crystallized subgrains, the model of Bischoff and Stöffler (1984) requires that the completely fused plagioclase maintains

a crystallographic "memory" of the parental grain, such that each newly crystallised subgrain re-assumes this identical crystallographic orientation. Bischoff and Stöffler admit that such a "memory" is at odds with experimental evidence.

At Popigai, the checkerboard texture is present in both plagioclase and pyroxene clasts. However, important compositional and mineralogical differences from those observed at Lappajärvi are inconsistent with an origin by fractional crystallisation of a fused clast. We prefer a model in which the texture is, instead, produced by crystallographically controlled partial melting of the clasts.

However, at Popigai, melt within the channels in the checkerboard plagioclase and pyroxenes is dissimilar to that expected from fusion of the host crystal. Instead, it is identical to that of the surrounding mesostasis melt. As a result, phases such as enstatite have grown from the melt in checkerboard plagioclases, which could not have crystallized from a melt derived by simple *in situ* melting of the feldspar. Alkali feldspar, minor pyroxene and opaques have also been noted in melt within checkerboard plagioclases from Manicouagan impact melt rocks (Simonds *et al.*, 1978). Although an explanation of their provenance was not offered, they are clearly not derived from the crystallisation of a plagioclase melt. Similarly, volumes of up to 20% plagioclase have crystallized from melt in checkerboard pyroxene. This plagioclase cannot have grown unless locally-derived pyroxene melts were significantly modified by the introduction of the Ca and Al, or the pyroxene melts were forcibly replaced by groundmass melt.

If the composition of the melt glass in the checkerboard clasts was modified by chemical diffusion from the groundmass melt into the checkerboard clast (*e.g.*, Sazonova and Korotaeva, 1989), compositional gradients would be expected from rim to core. However, no gradients are present. In addition, immiscible pyrrhotite droplets present in the mesostasis of some samples are also found in melt channels in the accompanying checkerboard pyroxene. Since there are no inclusions of sulfide in the unmelted pyroxene from which the sulfide droplets could have been derived, this provides the most compelling evidence that these droplets and the melt were injected from the surrounding mesostasis, thereby flushing the locally derived pyroxene melt during its passage.

Secondary growth of compositionally identical orthopyroxene on the relic, unmelted pyroxene subgrains subsequent to the main melting episode has resulted in a subhedral form to the subgrains (Fig. 8c). In the absence of such secondary pyroxene growth, the subgrains would be expected to possess embayed, anhedral forms. Secondary plagioclase growth from melt in checkerboard plagioclases produces similar subhedral subgrains (Fig. 7).

Checkerboard plagioclases and pyroxenes possess the same compositional ranges as their unmelted equivalents, indicating that clast melting is not controlled by composition. The presence of all textural varieties of plagioclase, including unmelted clasts in a single sample, also indicates that clast melting was not simply induced by heat from the surrounding impact melt, which would tend to produce a more uniform melting of the clasts. The partial melting must therefore have occurred prior to mixing, as a result of shock heating of minerals in the target, prior to their fragmentation and incorporation in the melt.

Calcic plagioclase mantles commonly occur on the partially-melted checkerboard feldspars and bridge the melt channels. This indicates that these overgrowths developed after the partial melting of the clasts. Locally, this mantle is missing along some external edges of broken clasts indicating that these clasts were broken by continued, localized turbulence of the melt, possibly during later stage processes. The presence of checkerboard and unmelted clasts, and unshocked and highly shocked quartz clasts in single samples, indicates that the impact melts have mixed clasts that have experienced vastly different shock conditions. Forcible injection of melt into the partially melted checkerboard clasts likely occurred during this turbulent mixing.

Although broken plagioclase overgrowth rims are not common, they do not appear to occur in samples in which glass clasts or globules are also found. This observation is consistent with the globular and glass fragments having been homogenized with the bulk melt during the turbulence responsible for fragmenting the plagioclases.

Lithic igneous clasts, containing both quartz and feldspar in the impact melt rocks at Lappajärvi, have been used to determine the type of shock effects that are generated in plagioclase for a given shock level, as indicated by the shock effects exhibited by co-existing quartz (Bischoff and Stöffler, 1984). At Lappajärvi, checkerboard plagioclases accompany clear and "toasted" quartz with PDFs, whereas totally recrystallized plagioclases accompany well-developed ballen-textured quartz. However, in quartz-plagioclase-bearing lithic clasts in the Popigai melt rocks, fine-grained, acicular recrystallized plagioclases with random orientations accompany "toasted" quartz, with PDFs but no ballen textures. This suggests that recrystallisation of the plagioclases can occur at lower shock levels than those that generate the ballen texture (<30 GPa). As such, it is probable that the pervasively recrystallised plagioclases replace diaplectic glass rather than fusion glass, which is typically only generated at shock pressures of ≥45–50 GPa.

Melt Homogenization and Preserved Heterogeneities

The homogeneity of major and the non-REE trace elements implies that the target rocks that melted to form the impact melts were either compositionally homogeneous, or that a heterogeneous suite of target rocks was well homogenized by the mixing that occurred during the crater excavation and modification stages. However, the slight variability in the concentration of the REE suggests that some heterogeneity from the target is preserved. Such variability may be a result

of local heterogeneities in the abundances of assimilated REE-hosting trace minerals in the impact melt rocks.

The isotopic differences noted between the glass and felsic clasts, the glass coatings on ejected gneiss bombs (Kettrup *et al.*, 2001), and the melt rocks, are likely a result of the degree of homogenisation: the melt rocks represent a more compositionally and isotopically homogenized mix of heterogeneous basement gneisses, while the clasts and glasses coating gneiss bombs preserve some of the heterogeneity of the target and may be derived from sedimentary rocks, with a Proterozoic basement provenance. The comparatively high volatility of Rb compared with Sr should lead to preferential Rb loss during impact vaporization of the target (and higher T(UR)Sr ages). However, glasses both depleted and enriched in Rb occur on the gneiss bombs. Consequently, we believe that it is unlikely that vaporization and condensation processes have generated these heterogeneities (cf., Kettrup *et al.*, 2001).

The non-uniform distribution of carbon in the samples may be related to the heterogeneous distribution of graphite, from which impact diamonds were generated, or a variable content of assimilated carbonate clasts, which are abundant in the target area, but are uncommon as preserved clasts.

Acknowledgments–The samples and a generous supply of knowledge and hospitality were offered to J. W. and R. A. F. G. by Victor Masaitis, Tanya Selivanovskaya and Anatoly Raikhlin while in St. Petersberg. We thank Amanda Amey for image analysis of the photomicrographs and Mike Dence for useful discussions with J. W. Microprobe analysis and scanning electron imagery were performed at UNB's Electron Microscopy Unit, with the assistance of Douglas Hall. Dimitri Papanastassiou, Gerry Wasserburg and Henry Ngo were very gracious hosts while the isotope measurements at Caltech were being gathered. Graham Nickerson of Interactive Visualization Systems was invaluable in the processing of the digital elevation data for the map insert. This work is funded by NSERC grants awarded to J. G. S. and R. A. F. G., and by the Barringer Crater Company, who supported J. W.'s visit to St. Petersburg. Contribution from the Geological Survey of Canada No. 2001099. UNB Planetary and Space Science Contribution No. 22.

Editorial handling: P. H. Warren

REFERENCES

BISCHOFF A. AND STÖFFLER D. (1984) Chemical and structural changes induced by thermal annealing of shocked feldspar inclusions in impact melt rocks from Lappajärvi crater, Finland. *J. Geophys. Res.* **89 (Suppl.)**, B645–B656.

BOTTOMLEY R., GRIEVE R., YORK D. AND MASAITIS V. (1997) The age of the Popigai impact event and its relation to events at the Eocene/Oligocene boundary. *Nature* **388**, 365–368.

CARSTENS H. (1975) Thermal history of impact melt rocks in the Fennoscandian Shield. *Contrib. Mineral. Petrol.* **50**, 145–155.

CLAEYS P., HEUSCHKEL S., ROCCHIA R., ROBIN E. AND STÖFFLER D. (1998) The two different melt rocks of the Chicxulub impact crater and where is the Ir anomaly? (abstract). *Lunar Planet. Sci.* **29**, #1361, Lunar and Planetary Institute, Houston, Texas, USA (CD-ROM).

DEER W. A., HOWIE R. A. AND ZUSSMAN J. (1992) *An Introduction to the Rock-Forming Minerals, 2nd Edition.* Longman Scientific and Technical, Essex, U.K. 695 pp.

VON ENGELHARDT W. (1972) Shocked produced glasses from the Ries crater. *Contrib. Mineral. Petrol.* **36**, 80–111.

FLORAN R. J., GRIEVE R. A. F., PHINNEY W. C., WARNER J. L., SIMONDS C. H., BLANCHARD D. P. AND DENCE M. R. (1978) Manicouagan impact melt, Quebec. 1: Stratigraphy, petrology and chemistry. *J. Geophys. Res.* **83**, 2737–2759.

FRENCH B. M. (1998) *Traces of Catastrophe: A Handbook of Shock-Metamorphic Effects in Terrestrial Meteorite Impact Structures.* L.P.I. Contribution No. **954**, Lunar and Planetary Institute, Houston, Texas, USA. 120 pp.

GRIEVE R. (1975) Petrology and chemistry of the impact melt at Mistastin lake crater, Labrador. *Geol. Soc. Am. Bull.* **86**, 1617–1629.

GRIEVE R. A. F. (1978) The melt rocks at the Brent Crater, Ontario, Canada. *Proc. Lunar Planet. Sci. Conf.* **9th**, 2579–2608.

GRIEVE R. A. F. AND FLORAN R. J. (1978) Manicouagan impact melt, Quebec. 2: Chemical interrelations with basement and formational processes. *J. Geophys. Res.* **83**, 2761–2771.

GRIEVE R. A. F., RUPERT J., SMITH J. AND THERRIAULT A. (1995) The record of terrestrial impact cratering. *GSA Today* **5**, 193–196.

GRIEVE R. A. F., LANGENHORST F. AND STÖFFLER D. (1996) Shock metamorphism of quartz in nature and experiment: II. Significance in geoscience. *Meteorit. Planet. Sci.* **31**, 6–35.

HÖLKER TH., DEUTSCH A. AND MASAITIS V. L. (1997) Nd-Sr Isotope signatures of impactites from the Popigai impact crater (Russia) (abstract). *Lunar Planet. Sci.* **28**, #1356, Lunar and Planetary Institute, Houston, Texas, USA (CD-ROM).

KALLEMEYN G. W., RUBIN A. E., WANG D. AND WASSON J. T. (1989) Ordinary chondrites: Bulk compositions, classification, lithophile-element fractionations, and composition-petrographic type relationships. *Geochim. Cosmochim. Acta* **53**, 2747–2767.

KALLEMEYN G. W., RUBIN A. E. AND WASSON J. T. (1991) The compositional classification of chondrites: V. The Karoonda (CK) group of carbonaceous chondrites. *Geochim. Cosmochim. Acta* **55**, 881–892.

KALLEMEYN G. W., RUBIN A. E. AND WASSON J. T. (1994) The compositional classification of chondrites: VI. The CR carbonaceous chondrite group. *Geochim. Cosmochim. Acta* **58**, 2873–2888.

KEITH H. D. AND PADDEN F. J., JR. (1963) A phenomenological theory of spherulite growth. *J. Appl. Phys.* **34**, 2409–2421.

KETTRUP B., DEUTSCH A. AND MASAITIS V. L. (2001) Sr, Nd isotope composition of impact melt coated gneiss bombs and tagamites, Popigai crater, Russia (abstract). *Lunar Planet. Sci.* **32**, #1290, Lunar and Planetary Institute, Houston, Texas, USA (CD-ROM).

KOEBERL C., MASAITIS V. L., SHAFRANOVSKY G. I., GILMOUR I., LANGENHORST F. AND SCHRAUDER M. (1997) Diamonds from the Popigai impact structure, Russia. *Geology* **25**, 967–970.

KRING D. A. AND BOYNTON W. V. (1992) Petrogenesis of an augite-bearing melt rock in the Chicxulub structure and its relationship to K/T impact spherules in Haiti. *Nature* **258**, 141–144.

LANGENHORST F. AND DEUTSCH A. (1994) Shock experiments on pre-heated α- and β-quartz: I. Optical and density data. *Earth Planet. Sci. Lett.* **128**, 683–698.

MASAITIS V. L. (1994) Impactites of the Popigai Impact Crater. In *Large Meteorites and Planetary Evolution* (eds. B. O. Dressler, R. A. F. Grieve and V. L. Sharpton), pp. 153–162. Geol. Soc. Am. Spec. Paper **293**, Geol. Soc. Am., Boulder, Colorado, USA.

MASAITIS V. L. AND RAIKHLIN A. I. (1986) The Popigai crater formed by the impact of common chondrite (in Russian). *Rep. Acad. Sci. USSR* **286**, 1476–1478.

MASAITIS V. L., FUTERGENDLER S. I. AND GNEVUSHEV M. A. (1972) Diamonds in impactites of the Popigai meteorite crater (in Russian). *Zapiski Vsesoyuznoge Mineralogicheskogo Obshchestva* **101**, 108–112.

MASAITIS V. L., MASHCHAK M. S., RAIKHLIN A. I. AND DANILIN A. N. (1980) The Popigai Astrobleme. In *The Geology of Astroblemes* (ed. Yu. E. Pogrebitsky), pp. 114–130. Nedra Press, Leningrad, Russia.

MASAITIS V. L., MASHCHAK M. S., RAIKLIN A. I., SELIVANOVSKAYA T. V. AND SHAFRANOVSKY G. I. (1998) *Diamond-Bearing Impactites of the Popigai Astrobleme.* VSEGEI Press, St. Petersburg, Russia. 179 pp.

MASAYTIS V. L., MIKHAILOV M. V. AND SELIVANOVSKAYA T. V. (1972) The Popigay meteorite crater. *Intl. Geol. Rev.* **14**, 327–331.

MCBIRNEY A. R. (1979) Effects of assimilation. In *The Evolution of the Igneous Rocks, Fiftieth Anniversary Perspectives* (ed. H. S. Yoder, Jr.), pp. 307–338. Princeton University Press, New Jersey, USA.

MCCORMICK K. A., TAYLOR G. J., KEIL K., SPUDIS P. D., GRIEVE R. A. F. AND RYDER G. (1989) Sources of clasts in terrestrial impact melts: Clues to the origin of LKFM. *Proc. Lunar Planet. Sci. Conf.* **19th**, 691–696.

MITTLEFEHLDT D. W., MCCOY T. M., GOODRICH C. A. AND KRACHER A. (1998) Non-chondritic meteorites from asteroidal bodies. In *Planetary Materials* (ed. J. J. Papike), pp. 4-04 to 4-195. Rev. Mineralogy **36**, Am. Mineral. Soc., Washington, D.C., USA.

POLSKY C. H. AND MCHONE J. F. (1998) Raman spectroscopic confirmation of metastable cristobalite in melt samples from the Wanapitei impact structure (abstract). *Lunar Planet. Sci.* **29**, #1471, Lunar and Planetary Institute, Houston, Texas, USA (CD-ROM).

REIMOLD W. U. (1982) The Lappajärvi meteorite crater, Finland: Petrography, Rb-Sr, major and trace element geochemistry of impact melt and basement rocks. *Geochim. Cosmochim. Acta* **46**, 1203–1225.

SATO H. (1975) Diffusion coronas around quartz xenocrysts in andesite and basalt from Tertiary volcanic region in northeastern Shikoku, Japan. *Contrib. Mineral. Petrol.* **50**, 49–64.

SAZONOVA L. V. AND KOROTAEVA N. N. (1989) Chemical diaplectic changes of plagioclases from impactites (Popigai and Puchezh-Katunk astroblemes, USSR) (abstract). *Meteoritics* **24**, 323.

SHORT N. M. AND GOLD D. P. (1996) Petrography of shocked rocks from the central peak at the Manson impact structure. In *The Manson Impact Structure, Iowa: Anatomy of an Impact Crater* (eds. C. Koeberl and R. R. Anderson), pp. 245–265. Geol. Soc. Am. Spec. Paper **302**, Geol. Soc. Am., Boulder, Colorado, USA.

SIMONDS C. H., FLORAN R. J., MCGEE P. E., PHINNEY W. C. AND WARNER J. L. (1978) Petrogenesis of melt rocks, Manicouagan impact structure, Quebec. *J. Geophys. Res.* **83**, 2773–2788.

SPUDIS P. D., RYDER G., TAYLOR G. J., MCCORMICK K. A., KEIL K. AND GRIEVE R. A. F. (1991) Sources of mineral fragments in impact melts 15445 and 15455: Toward the origin of low-K Fra Mauro basalt. *Proc. Lunar Planet. Sci. Conf.* **21st**, 151–165.

STECHER O., NGO H. H., PAPANASTASSIOU D. A. AND WASSERBURG G. J. (1989) Nd and Sr isotopic evidence for the origin of tektite material from DSDP site 612 off the New Jersey coast. *Meteoritics* **24**, 89–98.

STÖFFLER D. (1984) Glasses formed by hypervelocity impact. *J. Non-Cryst. Solids* **67**, 465–502.

STÖFFLER D. AND LANGENHORST F. (1994) Shock metamorphism of quartz in nature and experiment: 1. Basic observation and theory. *Meteoritics* **29**, 155–181.

TAYLOR S. R. AND MCLENNAN S. M. (1985) *The Continental Crust: Its Composition and Evolution.* Blackwell, Oxford, U.K. 312 pp.

VISHNEVSKII S. A., KOVALEVA L. T. AND PAL'CHIK N. A. (1974) Coesite in the rocks of the Popigai structure (in Russian). *Geologiya i Geofizika* **15**, 140–145.

VISHNEVSKY S. A. (1996) Two groups of Popigai impact glasses: A result of initial water content in target rocks. *Chimie der Erde* **56**, 493–497.

VISHNEVSKY S. AND MONTANARI A. (1999) Popigai impact structure (Arctic Siberia, Russia): Geology, petrology, geochemistry, and geochronology of glass-bearing impactites. In *Large Meteorite Impacts and Planetary Evolution II* (eds. B. O. Dressler and V. L. Sharpton), pp. 19–59. Geol. Soc. Am. Spec. Paper **339**, Geol. Soc. Am., Boulder, Colorado, USA.

VISHNEVSKY S. A., DOLGOV YU. A., KOVALEVA L. T. AND PAL'CHIK N. A. (1975) *Stishovite in Rocks of the Popigay Structure* (in Russian). Doklady Akademii Nauk SSSR **221**, 1167–1169.

WARREN P. H., CLAEYS P. AND CEDILLO-PARDO E. (1996) Mega-impact melt petrology (Chicxulub, Sudbury, and the Moon): Effects of scale and other factors on potential for fractional crystallization and development of cumulates. In *The Cretaceous–Tertiary Event and Other Catastrophes in Earth History* (eds. G. Ryder, D. Fastovovsky and S. Gartner), pp. 105–124. Geol. Soc. Am. Spec. Paper **307**, Geol. Soc. Am., Boulder, Colorado, USA.

WHITEHEAD J., PAPANASTASSIOU D. A., SPRAY J. G., GRIEVE R. A. F. AND WASSERBURG G. J. (2000) Late Eocene impact ejecta: Geochemical and isotopic connections with the Popigai impact structure. *Earth Planet. Sci. Lett.* **181**, 473–487.

WHITEHEAD J., SPRAY J. G. AND GRIEVE R. A. F. (2002). The origin of "toasted" quartz in meteorite impact structures. *Geology* (in press).